arXiv:1708.00757v1 [physics.plasm-ph] 21 Jul 2017

Spatially Localized Particle Energization by Landau Damping in Current Sheets Produced by Strong Alfvén Wave Collisions

GREGORY G. HOWES[1]†, ANDREW J. MCCUBBIN[1], and KRISTOPHER G. KLEIN[2]

[1]Department of Physics and Astronomy, University of Iowa, Iowa City, IA 52242, USA

[2]Department of Climate and Space Sciences and Engineering, University of Michigan, Ann Arbor, MI 48109, USA

(Received ?; revised ?; accepted ?.)

Understanding the removal of energy from turbulent fluctuations in a magnetized plasma and the consequent energization of the constituent plasma particles is a major goal of heliophysics and astrophysics. Previous work has shown that nonlinear interactions among counterpropagating Alfven waves—or Alfven wave collisions—are the fundamental building block of astrophysical plasma turbulence and naturally generate current sheets in the strongly nonlinear limit. A nonlinear gyrokinetic simulation of a strong Alfven wave collision is used to examine the damping of the electromagnetic fluctuations and the associated energization of particles that occurs in self-consistently generated current sheets. A simple model explains the flow of energy due to the collisionless damping and the associated particle energization, as well as the subsequent thermalization of the particle energy by collisions. The net particle energization by the parallel electric field is shown to be spatially intermittent, and the nonlinear evolution is essential in enabling that spatial non-uniformity. Using the recently developed field-particle correlation technique, we show that particles resonant with the Alfven waves in the simulation dominate the energy transfer, demonstrating conclusively that Landau damping plays a key role in the spatially intermittent damping of the electromagnetic fluctuations and consequent energization of the particles in this strongly nonlinear simulation.

1. Introduction

The space and astrophysical plasmas that fill the heliosphere, and other more remote astrophysical environments, are found generally to be both magnetized and turbulent. Understanding the removal of energy from turbulent fluctuations in a magnetized plasma and the consequent energization of the constituent plasma particles is a major goal of heliophysics and astrophysics. Although plasma heating and particle energization are governed by microscopic processes typically occurring at kinetic length scales in the plasma, these important energy transport mechanisms can have a significant impact on the macroscopic evolution of the systems. For example, the diffuse plasma of the solar corona is found to be nearly three orders of magnitude hotter than the solar photosphere. The dissipation of turbulent fluctuations, through a physical mechanism that is poorly understood at present, is believed to be responsible for this dramatic heating of the coronal plasma. This very high coronal temperature leads to the supersonic solar wind that pervades the entire heliosphere (Parker 1958), so the kinetic plasma physics governing

† Email address for correspondence: gregory-howes@uiowa.edu

the heating of the coronal plasma at small scales indeed impacts the global structure of the heliosphere.

The low density and high temperature conditions of the plasma in many astrophysical systems lead to a mean free path for collisions among the constituent charged particles that is often much longer than the length scales of the turbulent fluctuations. Under such weakly collisional plasma conditions, the dynamics of the turbulence and its dissipation is governed by kinetic plasma physics. Unlike in the more well-known case of fluid systems (which corresponds to the strongly collisional regime), in weakly collisional plasmas, the dissipation of turbulent energy into plasma heat is inherently a two-step process (Howes 2017). First, energy is removed from the turbulent electromagnetic fluctuations through collisionless interactions between the fields and particles, transferring that energy to non-thermal fluctuations in the particle velocity distribution functions, a process that is reversible. Subsequently, arbitrarily weak collisions can smooth out the small fluctuations in velocity space, leading to entropy increase and irreversible heating of the plasma (Howes *et al.* 2006; Howes 2008; Schekochihin *et al.* 2009). In this two-step process, the removal of energy from turbulent fluctuations and the subsequent conversion of that energy into plasma heat may even occur at different locations (Navarro *et al.* 2016).

In fluid simulations of plasma turbulence using the magnetohydrodynamic (MHD) approximation—a strongly collisional limit of the large-scale dynamics (relative to the characteristic kinetic plasma length scales)—the nonlinear evolution leads to the development of intermittent current sheets (Matthaeus & Montgomery 1980; Meneguzzi *et al.* 1981). Furthermore, it has been found that the dissipation of turbulent energy is largely concentrated in these intermittent current sheets (Uritsky *et al.* 2010; Osman *et al.* 2011; Zhdankin *et al.* 2013). Numerous studies have recently sought evidence for the spatial localization of plasma heating by the dissipation of turbulence in current sheets through statistical analyses of solar wind observations (Osman *et al.* 2011; Borovsky & Denton 2011; Osman *et al.* 2012; Perri *et al.* 2012; Wang *et al.* 2013; Wu *et al.* 2013; Osman *et al.* 2014) and numerical simulations (Wan *et al.* 2012; Karimabadi *et al.* 2013; TenBarge & Howes 2013; Wu *et al.* 2013; Zhdankin *et al.* 2013).

The mechanisms of the spatially localized dissipation found in MHD simulations are resistive (Ohmic) heating and viscous heating (Zhdankin *et al.* 2013; Brandenburg 2014; Zhdankin *et al.* 2015). But, resistivity and viscosity arise from microscopic collisions in the strongly collisional (or small mean free path) limit, a limit that is not applicable to the dynamics of dissipation in many space and astrophysical environments (Howes 2017). Under the weakly collisional conditions appropriate for most space and astrophysical plasmas, which physical mechanisms are responsible for the damping of the turbulent fluctuations and the consequent energization of the plasma particles remains an open question. Our aim here is to identify the mechanisms governing the damping of the turbulent fluctuations and the particle energization using a kinetic simulation code that follows the three-dimensional evolution of a weakly collisional plasma in which current sheets develop self-consistently.

Early research on incompressible MHD turbulence in the 1960s (Iroshnikov 1963; Kraichnan 1965) emphasized the wave-like nature of turbulent plasma motions, suggesting that nonlinear interactions between counterpropagating Alfvén waves—or simply *Alfvén wave collisions*—mediate the turbulent cascade of energy from large to small scales. In fact, the physics of the nonlinear interactions among Alfvén waves provides the foundation for modern scaling theories of plasma turbulence that explain the anisotropic nature of the turbulent cascade (Goldreich & Sridhar 1995) and the dynamic alignment of velocity and magnetic field fluctuations (Boldyrev 2006).

Following a number of previous investigations of weak incompressible MHD turbulence

(Sridhar & Goldreich 1994; Ng & Bhattacharjee 1996; Galtier *et al.* 2000), the nonlinear energy transfer in Alfvén wave collisions in the weakly nonlinear limit has been solved analytically (Howes & Nielson 2013), confirmed numerically with gyrokinetic numerical simulations (Nielson *et al.* 2013), and verified experimentally in the laboratory (Howes *et al.* 2012, 2013; Drake *et al.* 2013), establishing Alfvén wave collisions as the fundamental building block of astrophysical plasma turbulence. More recent research has found that Alfvén wave collisions in the strongly nonlinear limit naturally generate current sheets (Howes 2016), providing a first-principles explanation for the ubiquitous development of intermittent current sheets in plasma turbulence. This self-consistent generation of current sheets is found to persist even in the more realistic case of strong collisions between localized Alfvén wave packets (Verniero *et al.* 2017).

Here we explore the damping of the electromagnetic fluctuations and the associated energization of particles that occurs in current sheets that are generated self-consistently by strong Alfvén wave collisions. Previous work using a simulation of kinetic Alfvén wave turbulence has shown that, although enhanced plasma heating rates are well correlated with the presence of current sheets, the rate of heating as a function of wavenumber is well predicted assuming that linear Landau damping is entirely responsible for the removal of energy from the turbulence (TenBarge & Howes 2013). This result suggests that the physical mechanism governing the removal of energy from turbulent fluctuations, even in spatially intermittent current sheets, is Landau damping. Using nonlinear gyrokinetic simulations of strong Alfvén wave collisions, we aim to answer two questions:

(i) Is the dissipation associated with current sheets that are generated by strong Alfven wave collisions spatially intermittent?

(ii) What is the physical mechanism governing the removal of energy from the turbulence and the consequent energization of the particles?

2. Simulation

Similar to a previous study showing the development of current sheets in strong Alfvén wave collisions (Howes 2016), we employ the Astrophysical Gyrokinetics code `AstroGK` (Numata *et al.* 2010) to perform a gyrokinetic simulation of the nonlinear interaction between two counterpropagating Alfvén waves in the strongly nonlinear limit. `AstroGK` evolves the perturbed gyroaveraged distribution function $h_s(x, y, z, \lambda, \varepsilon)$ for each species s, the scalar potential φ, the parallel vector potential $A_\parallel$, and the parallel magnetic field perturbation $\delta B_\parallel$ according to the gyrokinetic equation and the gyroaveraged Maxwell's equations (Frieman & Chen 1982; Howes *et al.* 2006). Velocity space coordinates are $\lambda = v_\perp^2/v^2$ and $\varepsilon = v^2/2$. The domain is a periodic box of size $L_\perp^2 \times L_\parallel$, elongated along the straight, uniform mean magnetic field $\mathbf{B}_0 = B_0\hat{\mathbf{z}}$, where all quantities may be rescaled to any parallel dimension satisfying $L_\parallel/L_\perp \gg 1$. Uniform Maxwellian equilibria for ions (protons) and electrons are chosen, with a reduced mass ratio $m_i/m_e = 36$ such that, even with the modest spatial resolution of this simulation, the collisionless damping by ions and electrons is sufficiently strong within the resolved range of length scales to terminate the nonlinear transfer of energy to small scales. Spatial dimensions (x, y) perpendicular to the mean field are treated pseudospectrally; an upwind finite-difference scheme is used in the parallel direction, z. Collisions employ a fully conservative, linearized collision operator with energy diffusion and pitch-angle scattering (Abel *et al.* 2008; Barnes *et al.* 2009).

To set up the simulation of an Alfvén wave collision, following Nielson *et al.* (2013), we initialize two perpendicularly polarized, counterpropagating plane Alfvén waves, $\mathbf{z}^+ = z_+ \cos(k_\perp x - k_\parallel z - \omega_0 t)\hat{\mathbf{y}}$ and $\mathbf{z}^- = z_- \cos(k_\perp y + k_\parallel z - \omega_0 t)\hat{\mathbf{x}}$, where $\omega_0 = k_\parallel v_A$,

$k_\perp = 2\pi/L_\perp$, and $k_\parallel = 2\pi/L_\parallel$. Here $\mathbf{z}^\pm = \mathbf{u} \pm \delta\mathbf{B}/\sqrt{4\pi(n_i m_i + n_e m_e)}$ are the Elsasser fields (Elsasser 1950) which represent Alfvén waves that propagate up or down the mean magnetic field at the Alfvén velocity $v_A = B_0/\sqrt{4\pi(n_i m_i + n_e m_e)}$ in the MHD limit, $k_\perp \rho_i \ll 1$. We specify a balanced collision with equal counterpropagating wave amplitudes, $z_+ = z_-$, such that the nonlinearity parameter is $\chi = k_\perp z_\pm/(k_\parallel v_A) = 1$, relevant to the regime of strong turbulence (Goldreich & Sridhar 1995). To study the nonlinear evolution in the limit $k_\perp \rho_i \ll 1$, we choose a perpendicular simulation domain size $L_\perp = 8\pi\rho_i$ with simulation resolution $(n_x, n_y, n_z, n_\lambda, n_\varepsilon, n_s) = (64, 64, 32, 128, 32, 2)$. The fully resolved perpendicular range in this dealiased pseudospectral method covers $0.25 \leqslant k_\perp \rho_i \leqslant 5.25$, or $0.042 \leqslant k_\perp \rho_e \leqslant 0.875$ given the chosen mass ratio $m_i/m_e = 36$ and temperature ratio $T_i/T_e = 1$. Here the ion thermal Larmor radius is $\rho_i = v_{ti}/\Omega_i$, the ion thermal velocity is $v_{ti}^2 = 2T_i/m_i$, the ion cyclotron frequency is $\Omega_i = q_i B_0/(m_i c)$, and the temperature is given in energy units. The plasma parameters of the simulation are $\beta_i = 1$ and $T_i/T_e = 1$, typical of near-Earth solar wind conditions. The linearized Landau collision operator (Abel *et al.* 2008; Barnes *et al.* 2009) is employed with collisional coefficients $\nu_i = \nu_e = 6 \times 10^{-4} k_\parallel v_A$, yielding weakly collisional dynamics with $\nu_s/\omega \ll 1$.

To prepare the simulation, the two initial Alfvén wave modes are evolved linearly for five periods with enhanced collision frequencies $\nu_i = \nu_e = 0.01 k_\parallel v_A$ to eliminate any transient behavior arising from the initialization that does not agree with the properties of the Alfvén wave mode (Nielson *et al.* 2013). The simulation is then restarted with the nonlinear terms enabled, beginning the nonlinear evolution of the strong Alfvén wave collision. Note that the two Alfvén waves are already overlapping at the beginning of this simulation before the nonlinear evolution begins, an idealized case which facilitates the comparison to an asymptotic analytical solution in the weakly nonlinear limit (Howes & Nielson 2013; Howes 2016). The nonlinear evolution of development of current sheets is found to persist in the more realistic case of collisions between two initially separated Alfvén wavepackets of finite parallel extent (Verniero *et al.* 2017; Verniero & Howes 2017).

For the plasma parameters of this gyrokinetic simulation, we solve the linear collisionless gyrokinetic dispersion relation (Howes *et al.* 2006) for the Alfvén/kinetic Alfvén wave mode to determine the linear frequency and collisionless damping rate for this mode as a function of perpendicular wavenumber. Note that the collisionless damping of this mode is due to the Landau resonances with the ions and electrons. In the upper panel of Fig. 1 is plotted the normalized real frequency $\omega/k_\parallel v_A$ vs. the normalized perpendicular wavenumber $k_\perp \rho_i$. In the lower panel is plotted the total collisionless damping rate normalized to the wave frequency γ/ω (solid black), as well as the separate contributions to this linear collisionless damping rate from the ions (red dotted) and electrons (blue dashed). These gyrokinetic results have been verified by comparison with the solutions of the full Vlasov-Maxwell linear dispersion relation using the PLUME solver (Klein & Howes 2015). Since gyrokinetic theory resolves the Landau resonances but not the cyclotron resonances, this agreement between the gyrokinetic and the Vlasov-Maxwell results confirms that the linear collisionless damping is due to the Landau resonance.

Fig. 1 shows that the collisional damping by the ions (red dotted) has a relatively broad peak over the range $0.5 \lesssim k_\perp \rho_i \lesssim 2.0$. The range of resonant parallel phase velocities $\omega/k_\parallel$ associated with this broad peak in damping, normalized in terms of the ion thermal velocity, is $1.0 \lesssim \omega/k_\parallel v_{ti} \lesssim 1.5$. Therefore, if Landau damping with the ions is active, the energy transfer should be dominated by resonant ions with parallel velocities in the range $1.0 \lesssim v_\parallel/v_{ti} \lesssim 1.5$. The collisionless damping by the electrons, on the other hand, increases monotonically with perpendicular wavenumber, becoming sufficiently strong with $\gamma_e/\omega \gtrsim 0.1$ at $k_\perp \rho_i \gtrsim 1.2$. From this point, up to the maximum

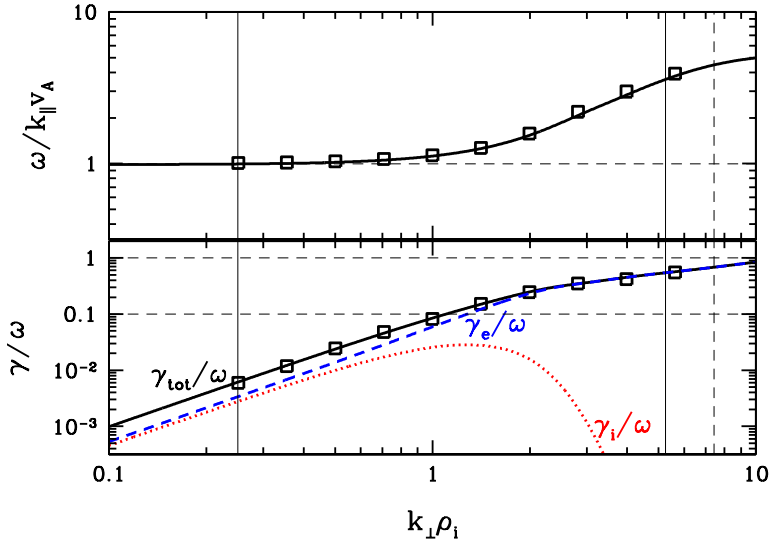


FIGURE 1. (a) The normalized frequency $\omega/k_\parallel v_A$ and (b) total collisionless damping rate γ_{tot}/ω (black solid) vs. $k_\perp\rho_i$ for Alfvén and kinetic Alfvén waves with $m_i/m_e = 36$ from the linear collisionless gyrokinetic dispersion relation, including the separate contributions to the linear collisionless damping rate from the ions γ_i/ω (red dotted) and the electrons γ_e/ω (blue dashed). Squares indicate values computed from linear runs of `AstroGK`. Solid vertical lines indicate the limits of the fully resolved perpendicular scales of the nonlinear simulation at $k_\perp\rho_i = 0.25$ and $k_\perp\rho_i = 5.25$. The vertical dashed line indicates the highest $k_\perp\rho_i$ value, $k_\perp\rho_i = 5.25\sqrt{2} \simeq 7.42$, of the modes in the corner of Fourier space.

fully resolved perpendicular scale of $k_\perp\rho_i = 5.25$, the range of resonant parallel phase velocities $\omega/k_\parallel$ in terms of the electron thermal velocity is $0.17 \lesssim \omega/k_\parallel v_{te} \lesssim 0.6$. Therefore, if the collisionless energy transfer from the turbulent electromagnetic fields to the plasma particles is governed by a Landau resonant mechanism, we would expect to see the transfer of energy localized at parallel velocities within this range of resonant values.

3. Evolution of Energy

Under weakly collisional plasma conditions typical of many heliospheric and astrophysical plasmas, the removal of energy from turbulent fluctuations and the eventual conversion of that energy into plasma heat, unlike in the more familiar fluid limit, is a two-step process (Howes 2017). Specifically, the turbulent fluctuations are first damped through reversible, collisionless interactions between the electromagnetic fields and the plasma particles, leading to energization of the particles. This non-thermal energization of the particle velocity distributions is subsequently thermalized by arbitrarily weak collisions, thereby accomplishing the ultimate conversion of the turbulent energy into particle heat. An analysis of the flow of energy in this Alfvén wave collision simulation illustrates these two distinct steps of the turbulent dissipation.

In a gyrokinetic system, the *total fluctuating energy* δW (Howes *et al.* 2006; Brizard & Hahm

2007; Schekochihin *et al.* 2009) is given by†

$$\delta W = \int d^3\mathbf{r} \left[\frac{|\delta\mathbf{B}|^2 + |\delta\mathbf{E}|^2}{8\pi} + \sum_s \int d^3\mathbf{v} \, \frac{T_{0s}\delta f_s^2}{2F_{0s}} \right], \tag{3.1}$$

where the index s indicates the plasma species and T_{0s} is the temperature of each species' Maxwellian equilibrium. The left term represents the electromagnetic energy and the right term represents that microscopic fluctuating kinetic energy of the particles of each plasma species s. Note that the elimination of the parallel nonlinearity in the standard form of gyrokinetic theory means that the appropriate conserved quadratic quantity in gyrokinetics is the Kruskal-Obermann energy, $E_s^{(\delta f)} \equiv \int d^3\mathbf{r} \int d^3\mathbf{v} \; T_{0s}\delta f_s^2/2F_{0s}$ (Kruskal & Oberman 1958; Morrison 1994), in contrast to the usual kinetic theory definition of microscopic kinetic energy, $\int d^3\mathbf{r} \int d^3\mathbf{v} \; (m_s v^2/2) f_s$. Note also that δW includes neither the equilibrium thermal energy, $\int d^3\mathbf{r} \frac{3}{2} n_{0s} T_{0s} = \int d^3\mathbf{r} \int d^3\mathbf{v} \frac{1}{2} m_s v^2 F_{0s}$, nor the equilibrium magnetic field energy, $\int d^3\mathbf{r} \; B_0^2/8\pi$. Thus, the terms of δW in (3.1) represent the perturbed electromagnetic field energies and the microscopic kinetic energy of the deviations from the Maxwellian velocity distribution for each species.

A more intuitive form of the total fluctuating energy δW can be obtained by separating out the kinetic energy of the bulk motion of the plasma species from the non-thermal energy in the distribution function that is not associated with bulk flows (Li *et al.* 2016),

$$\delta W = \int d^3\mathbf{r} \left[\frac{|\delta\mathbf{B}|^2 + |\delta\mathbf{E}|^2}{8\pi} + \sum_s \left(\frac{1}{2} n_{0s} m_s |\delta\mathbf{u_s}|^2 + \frac{3}{2}\delta P_s \right) \right] \tag{3.2}$$

where n_{0s} is the equilibrium density, m_s is mass, and $\delta\mathbf{u_s}$ is the fluctuating bulk flow velocity. The *non-thermal energy* in the distribution function (not including the bulk kinetic energy) is defined by $E_s^{(nt)} \equiv \int d^3\mathbf{r} \frac{3}{2}\delta P_s \equiv \int d^3\mathbf{r} (\int d^3\mathbf{v} \; T_{0s}\delta f_s^2/2F_{0s} - \frac{1}{2} n_{0s} m_s |\delta\mathbf{u_s}|^2)$ (TenBarge *et al.* 2014). The *turbulent energy* is defined as the sum of the electromagnetic field and the bulk flow kinetic energies (Howes 2015; Li *et al.* 2016), $E^{(turb)} \equiv \int d^3\mathbf{r} [(|\delta\mathbf{B}|^2 + |\delta\mathbf{E}|^2)/8\pi + \sum_s \frac{1}{2} n_{0s} m_s |\delta\mathbf{u_s}|^2]$. Therefore the total fluctuating energy is simply the sum of the turbulent energy and species non-thermal energies, $\delta W = E^{(turb)} + E_i^{(nt)} + E_e^{(nt)}$.

3.1. *Evolution of Turbulent and Non-Thermal Energies*

In Fig. 2, we plot the evolution of these three different contributions to the total fluctuating energy normalized to the total initial fluctuating energy $\delta W_0 \equiv \delta W(t = 0)$. In Fig. 2(a), we plot the total fluctuating energy $\delta W/\delta W_0$ (black), the turbulent energy $E^{(turb)}/\delta W_0$ (purple), the ion non-thermal energy $E_i^{(nt)}/\delta W_0$ (red), and the electron non-thermal energy $E_e^{(nt)}/\delta W_0$ (blue). Note that collisions in `AstroGK`, as well as in real plasma systems, convert non-thermal to thermal energy, representing irreversible plasma heating with an associated increase of entropy. The energy lost from δW by collisions is tracked by `AstroGK` and represents thermal heating of the plasma species, but this energy is not fed back into the code to evolve the equilibrium thermal temperature, T_{0s} (Howes *et al.* 2006; Numata *et al.* 2010; Li *et al.* 2016). The evolution in Fig. 2(a) makes clear that, over 7.5 periods of the initial Alfvén waves, more than 60% of the initial fluctuating energy in the simulation is lost to collisional heating.

In Fig. 2(b), we plot the different components that contribute to the turbulent energy

† Note that in the gyrokinetic approximation, the electric field energy is relativistically small relative to the magnetic field energy (Howes *et al.* 2006).

$E^{(turb)}$. In order of decreasing magnitude, these contributions are the perpendicular magnetic energy $E_{B_\perp}$ (green dashed), perpendicular ion kinetic energy $E_{u_{i,\perp}}$ (red dashed), perpendicular electron kinetic energy $E_{u_{e,\perp}}$ (blue dashed), parallel magnetic energy $E_{B_\parallel}$ (green dotted), parallel ion kinetic energy $E_{u_{i,\parallel}}$ (red dotted), and parallel electron kinetic energy $E_{u_{e,\parallel}}$ (blue dotted). The turbulent energy is dominated by the perpendicular magnetic energy and perpendicular ion kinetic energy. This is expected for Alfvénic fluctuations at $k_\perp \rho_i \ll 1$: transverse motion of the plasma dominated by ion kinetic energy is first arrested by magnetic tension, followed by the acceleration of the plasma back toward the equilibrium point by magnetic tension, thereby leading to the oscillatory transfer of energy back and forth between perpendicular magnetic energy and perpendicular ion kinetic energy, as evident in Fig. 2(b). Note that this energy is integrated over the entire simulation domain, so neither of these energies is expected to drop to zero, as would occur for the energy density at a single point in space as an Alfvén wave passes through that point. In the MHD limit $k_\perp \rho_i \ll 1$, Alfvénic fluctuations also have very little parallel motion, $u_\parallel \ll u_\perp$ and a very small parallel magnetic field fluctuation, $\delta B_\parallel \ll \delta B_\perp$. Finally, the electron kinetic energies are down from the respective ion kinetic energies approximately by a factor of the mass ratio, $m_e/m_i = 1/36$, so electrons make a subdominant contribution to the turbulent energy. Finally, note that although the volume integrated energy of each component of $E^{(turb)}$ shows oscillations with the period T_0, their sum varies smoothly in time, suggesting that this definition of turbulent energy is physically well motivated.

3.2. *Evolution of Collisional Heating*

In Fig. 3, we present the evolution of the collisional heating rate per unit volume of ions Q_i (red) and electrons Q_e (blue) as well as the total collisional heating rate $Q_{tot} = Q_i + Q_e$ (black) for this nonlinear Alfvén wave collision simulation (thick lines). The heating rates are normalized by a characteristic heating rate per unit volume, $Q_0 = (n_{0i} T_{0i} v_{ti}/L_\parallel)(\pi/8)(L_\perp/L_\parallel)^2$. The total fluctuating energy δW in Fig. 2(a) diminishes in time due to thermalization by collisions. This collisional energy loss from δW is tracked in `AstroGK` by this collisional heating rate, enabling energy conservation to be measured in the simulation.

Note that the rapid initial rise in the collisional damping rate for the electrons Q_e at $t/T_0 \lesssim 0.5$ in Fig. 3 is due to the fact that the linear initialization uses higher collision coefficients, $\nu_s = 0.01 k_\parallel v_A$, than the subsequent nonlinear evolution, $\nu_s = 6 \times 10^{-4} k_\parallel v_A$. When the collisional coefficients are reduced, smaller velocity scale structures in the velocity distribution must develop (through the kinetic evolution) before the collisional heating is able to effectively thermalize the non-thermal energy contained in those fluctuations.

Also plotted in Fig. 3 is the evolution of the collisional heating rates in a linear simulation (thin lines), where the simulation is started from the same initial conditions but the nonlinear terms are turned off. In this linear simulation, there is no nonlinear transfer of energy to other Fourier modes—meaning that there is no nonlinear turbulent cascade of energy to small scales—so the evolution of the energy is solely due to linear Landau damping of the initial Alfvén waves and the subsequent collisional thermalization of the fluctuations in the velocity distribution functions that were generated by this linear Landau damping. It is important to note that the nonlinear evolution eventually leads to a higher collisional heating rate, presumably through the nonlinear transfer of energy to smaller scale fluctuations that have higher collisionless damping rates than the initial Alfvén waves, although we do not directly analyze that nonlinear cascade of energy in this study.

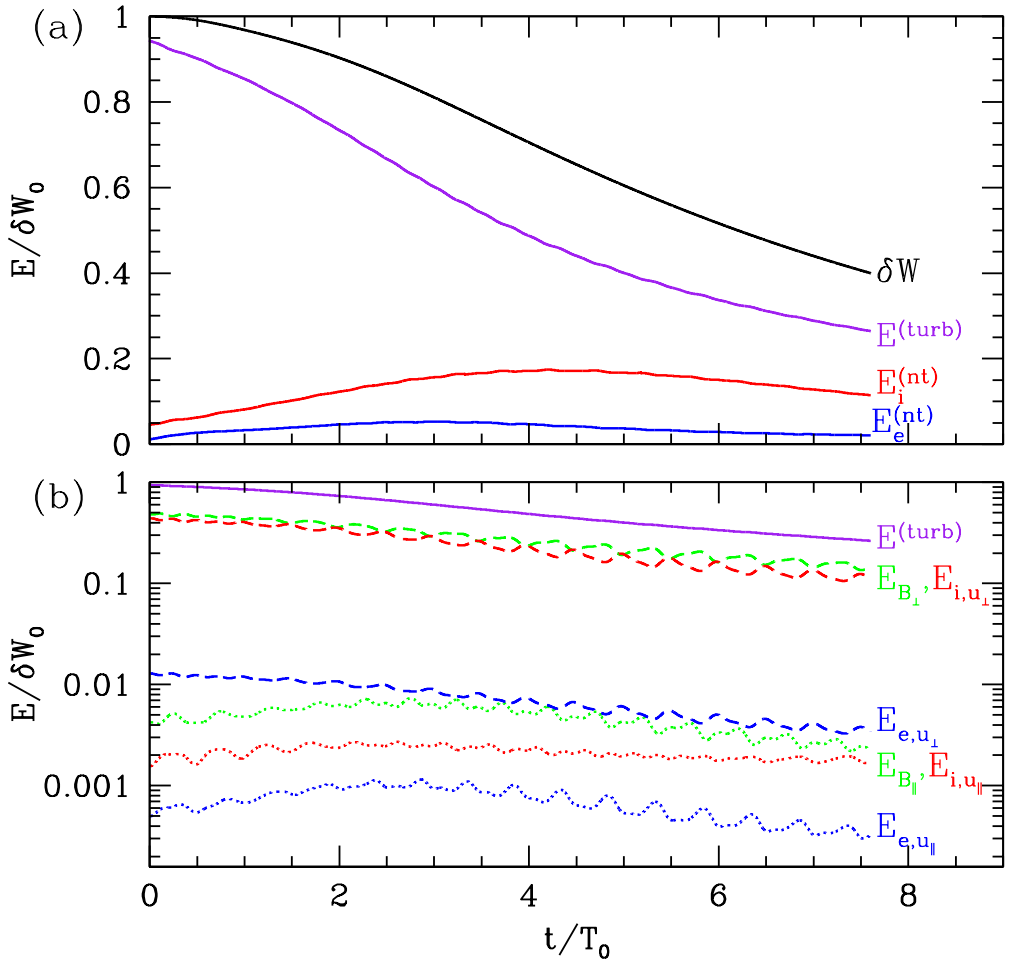


FIGURE 2. (a) Evolution of the normalized energy $E/\delta W_0$ as a function of time t/T_0 for the total fluctuating energy δW (black), the turbulent energy $E^{(turb)}$ (purple), the ion non-thermal energy $E_i^{(nt)}$ (red) and the electron non-thermal energy $E_e^{(nt)}$ (blue). (b) Evolution of the different components of the turbulent energy $E^{(turb)}$ (purple), dominated by the perpendicular magnetic field energy $E_{B_\perp}$ (green dashed) and the perpendicular ion bulk flow kinetic energy $E_{i,u_\perp}$ (red dashed), with successively smaller contributions by the perpendicular electron bulk kinetic energy $E_{e,u_\perp}$ (blue dashed), the parallel magnetic field energy $E_{B_\parallel}$ (green dotted), the parallel ion bulk flow kinetic energy $E_{i,u_\parallel}$ (red dotted), and the parallel electron bulk flow kinetic energy $E_{e,u_\parallel}$ (blue dotted).

3.3. *Model of Energy Flow*

A physical interpretation of the two-step energy flow in this strong Alfvén wave collision simulation is illustrated by the diagram in Fig. 4. The energy of turbulent fluctuations $E^{(turb)}$, consisting of the sum of the electromagnetic field fluctuations and the kinetic energy of the bulk flows (first velocity moment) of each plasma species (Howes 2015, 2017), can be removed by collisionless interactions $\dot{E}_s^{(fp)}$ between the electromagnetic fields and

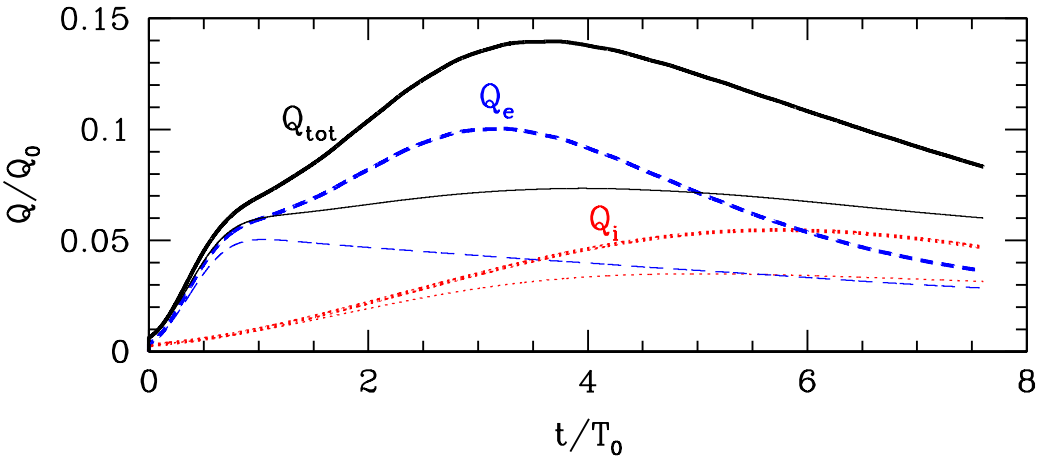


FIGURE 3. Ion collisional heating rate Q_i/Q_0 (red), electron collisional heating rate (blue) and total collisional heating rate $Q_{tot} = Q_i + Q_e$ (black) and as a function of time t/T_0 for the nonlinear simulation (thick lines). Also plotted (thin lines) is the linear evolution from the same initial conditions.

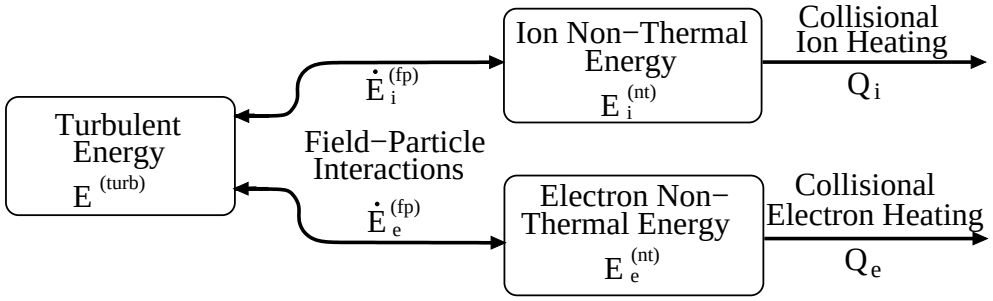


FIGURE 4. Diagram of the energy flow in weakly collisional turbulent plasmas, showing that interactions between the electromagnetic fields and plasma particles $\dot{E}_s^{(fp)}$ can reversibly transfer energy between the turbulent energy $E^{(turb)}$ and the non-thermal energy in the velocity distribution function of each species $E_s^{(nt)}$. Collisional heating Q_s then can irreversibly convert this non-thermal energy, represented by fluctuations in velocity space of each species, into heat of each plasma species s. This is the two-step process of reversible particle energization and subsequent irreversible thermalization of that particle energy.

the plasma particles. This energy is converted to non-thermal energy of the ions and electrons, $E_s^{(nt)}$. This non-thermal energy is represented by fluctuations in the particle velocity distribution functions that have no associated bulk flow (first moment), and therefore do not contribute to the turbulent motions. A key property of this collisionless energy transfer $\dot{E}_s^{(fp)}$ is that it is reversible (two-headed arrows in Fig. 4), representing the electromagnetic work done on the particles by the fields, which can be positive or negative.

The non-thermal energy $E_s^{(nt)}$ is contained in fluctuations in velocity-space of the particle velocity distribution functions for each species, $\delta f_s(\mathbf{v})$. If these fluctuations reach sufficiently small scales in velocity space, arbitrarily weak collisions can smooth out those fluctuations, thermalizing their energy and thereby realizing irreversible plasma heating, Q_s. The kinetic equation for each species governs two mechanisms that facilitate

the transfer of energy to ever smaller scales in velocity space: linear phase mixing and nonlinear phase mixing.

The first mechanism is linear phase mixing governed by the ballistic term in the kinetic equation, which couples spatial variations with velocity-space fluctuations and can lead to the transfer of energy to small scales in velocity space.† In linear Landau damping, for example, the energy of a damped wave is first transferred collisionlessly into non-thermal velocity space fluctuations, which subsequently phase mix linearly to small enough scales in velocity space that weak collisions can irreversibly convert the non-thermal energy into plasma heat. Boltzmann's H theorem proves that the entropy increase associated with irreversible plasma heating is ultimately collisional (Howes *et al.* 2006).

In addition to this linear phase-mixing process, at perpendicular spatial scales comparable to the particle thermal Larmor radii, $k_\perp \rho_s \gtrsim 1$, a nonlinear phase-mixing process (Dorland & Hammett 1993), also known as the entropy cascade (Schekochihin *et al.* 2009; Tatsuno *et al.* 2009; Plunk *et al.* 2010; Plunk & Tatsuno 2011; Kawamori 2013), can be very effective at transferring energy to ever smaller scales in velocity space. Ultimately, when the non-thermal particle energy in the velocity distribution functions $\delta f_s(\mathbf{v})$ has reached sufficiently small scales in velocity, due to some combination of linear and nonlinear phase mixing, collisions may thermalize that particle energy, completing the final step in the conversion of turbulent energy into plasma heat. In `AstroGK`, this collisional heating removes energy from fluctuating energy in the plasma, δW.

It is worthwhile to contrast this two-step mechanism in weakly collisional plasmas—collisionless particle energization followed by collisional thermalization—with the more familiar picture of turbulent dissipation in the fluid (strongly collisional) limit. A dimensionless measure of the collisionality is the ratio of the thermal collision rate to the frequency of typical fluctuations in the plasma, ν/ω. In the strongly collisional limit, $\nu/\omega \gg 1$, collisions can directly remove energy from both the bulk plasma flows through viscosity and the plasma currents through resistivity. Because both viscosity and resistivity are collisional, entropy increases through these mechanisms, and the energy from the turbulent electromagnetic field and plasma flow fluctuations is immediately thermalized to plasma heat. Thus, the dissipation of turbulence in the strongly collisional, fluid limit is a single-step process. Consider the example of resistive MHD, where Ohm's Law gives the electric field in terms of the plasma fluid velocity, magnetic field, and current density, $\mathbf{E} + \mathbf{U}/c \times \mathbf{B} = \eta \mathbf{j}$ (Spitzer 1962; Kulsrud 1983). The work done by the electric field is $\mathbf{j} \cdot \mathbf{E} = -\mathbf{j} \cdot (\mathbf{U}/c \times \mathbf{B}) + \eta \mathbf{j}^2$, where second term is the non-negative Ohmic heating due to resistive dissipation of the current, showing that the resistivity leads directly to plasma heating.

The strong Alfvén wave collision simulation presented here has $\nu/\omega \sim 6 \times 10^{-4} \ll 1$, firmly in the weakly collisional limit. Unlike in the MHD Ohm's Law above, where the current density $\mathbf{j}$ and electric field $\mathbf{E}$ due to the resistive term are in phase, and thereby yield a zero or positive change in energy, in the weakly collisional case the current density $\mathbf{j}$ and electric field $\mathbf{E}$ need not be in phase, enabling the work done by collisionless interactions between the fields and particles to give energy to or take energy from the particles. In fact, if the current and electric field are exactly 90 degrees out of phase, there is zero net energy transfer between fields and particles over one complete oscillation, corresponding to undamped wave motion. The bottom line, a point that

† It has been recently suggested that, under particular conditions in a turbulent plasma of sufficiently low collisionality, a turbulent anti-phase-mixing process can prevent velocity space fluctuations from reaching sufficiently small-scales to enable thermalization by collisions (Schekochihin *et al.* 2016; Parker *et al.* 2016).

cannot be overstated, is that in a weakly collisional plasma, the electromagnetic work $\mathbf{j} \cdot \mathbf{E}$ does not correspond to irreversible plasma heating, but rather to reversible work done on the particles by the fields, or vice versa.

Developing a detailed understanding of particle energization and plasma heating in heliospheric plasmas is grand challenge problem in heliophysics, and this simple model of the energy flow provides important constraints to focus efforts in that endeavor. Note that the final step of the process in Fig. 4, the thermalization of the particle energy, is fundamentally collisional, independent of what mechanism (which we have not specified here) removed energy from the turbulent fluctuations initially. The key question in understanding particle energization and plasma heating in heliospheric plasmas is therefore to understand the first step: what collisionless and reversible mechanism is responsible for the removal of energy from the turbulent fluctuations and conversion of that energy into non-thermal energy of the plasma species?

3.4. *Rate of Energy Transfer*

Now we use the strong Alfvén wave collision simulation presented here to analyze the channels of energy transfer shown in Fig. 4. For each species, the rate of change of non-thermal energy is given by

$$\dot{E}_s^{(nt)} = \dot{E}_s^{(fp)} - Q_s, \tag{3.3}$$

where the irreversible collisional heating $Q_s \geqslant 0$ but the reversible collisionless field-particle energy transfer $\dot{E}_s^{(fp)}$ can be either positive or negative. In addition, the rate of change of turbulent energy must be the sum of the collisionless field-particle energy transfer for each species,

$$-\dot{E}^{(turb)} = \dot{E}_i^{(fp)} + \dot{E}_e^{(fp)}. \tag{3.4}$$

Note that we have not specified the physical mechanism governing the field-particle energy transfer, but we are simply showing that the transfers of energy indeed follow the diagram in Fig. 4. The rate of field-particle energy transfer presented below is calculated from (3.3) as the difference between the rate of change of non-thermal particle energy and the collisional heating rate for each species.

In Fig. 5, we present the terms of these energy transfer relations for the (a) ions and (b) electrons, as well as (c) the balance between the loss of turbulent energy and the field-particle energy transfer to each species. A few very interesting aspects of Fig. 5 are worth highlighting. First, although the change of turbulent energy $E^{(turb)}$ and non-thermal energies $E_s^{(nt)}$ in Fig. 2 appears to be smooth, the time derivative, which gives the rate of change, indeed varies rapidly, including a significant fluctuation with period $T_0/2$.

Second, in Fig. 5(b), the energy transferred into electron non-thermal energy at the rate $\dot{E}_e^{(fp)}$ (solid) is very quickly thermalized by collisions into electron heat (dashed); the time lag between these two curves is $\Delta t = 0.6T_0$ (not shown), suggesting that non-thermal energy transferred into the electron velocity distribution is rapidly transferred by phase mixing to sufficiently small velocity-space scales to be thermalized by the weak collisions. For the ions in Fig. 5(a), on the other hand, the time lag between the energy transferred into non-thermal ion energy $\dot{E}_i^{(fp)}$ and the thermalization of that ion energy is approximately $\Delta t = 3.6T_0$, a factor of $\sqrt{m_i/m_e} = 6$ longer, suggesting that the phase-mixing occurs more slowly for ions by the ratio of the electron-to-ion thermal velocity. Note also that the collisionless field-particle energy transfer to ions indeed becomes negative at a few points in time, as allowed for a reversible process.

Furthermore, note that the magnitudes of $\dot{E}_i^{(fp)}$ and $\dot{E}_e^{(fp)}$ are fairly similar, as ex-

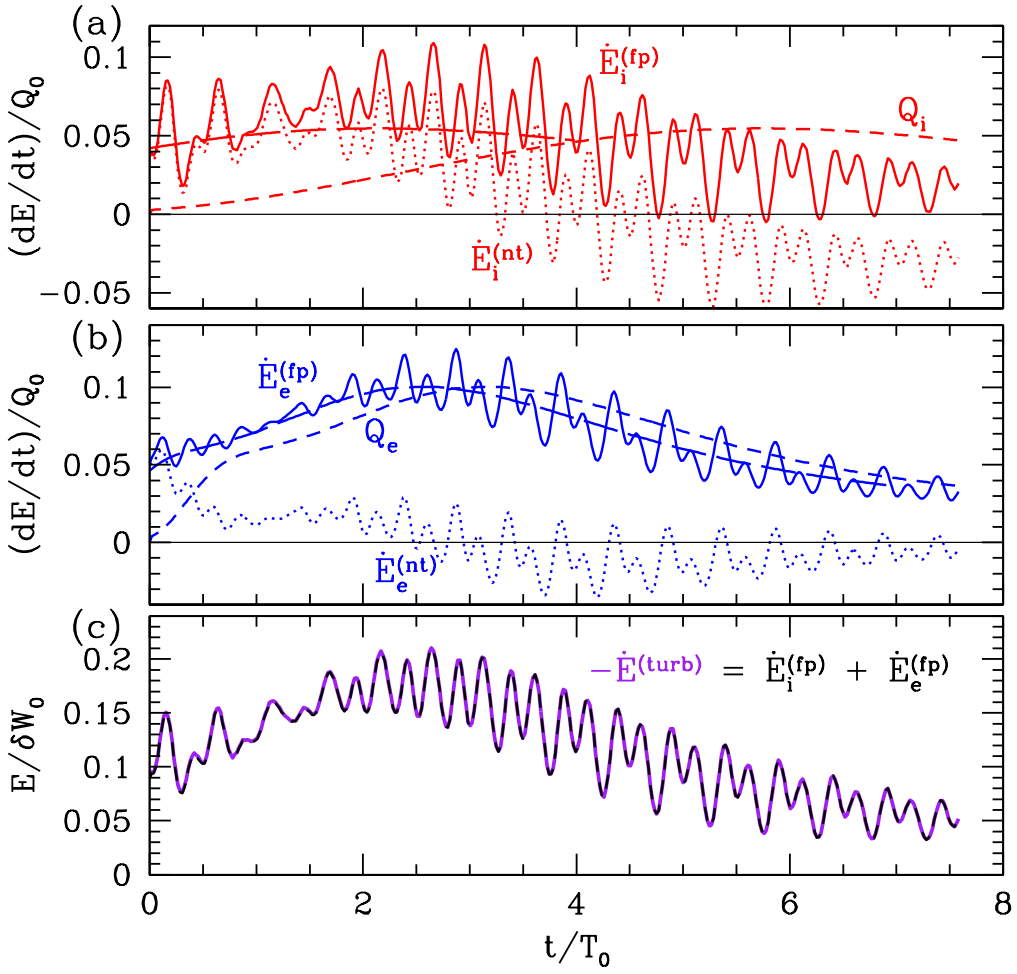


FIGURE 5. The rate of energy transfer by field-particle interactions $\dot{E}_s^{(fp)}$ (solid), the rate of change of non-thermal energy $\dot{E}_s^{(nt)}$ (dotted), and the collisional heating rate Q_s (dashed) for (a) ions (red) and (b) electrons (blue). (c) The energy balance between the loss of turbulent energy $-\dot{E}^{(turb)}$ (purple solid) and the summed transfer of energy to both ions and electrons, $\dot{E}_i^{(fp)} + \dot{E}_e^{(fp)}$ (black dashed).

pected because the linear damping rates, shown in Fig. 1, are fairly similar for ions and electrons, $\gamma_i \simeq \gamma_e$, over the range of spatial scales $k_\perp \rho_i < 1$ that contain most of the energy in the simulation. Finally, in Fig. 5(c), we see that the energy lost by the turbulence $-\dot{E}^{(turb)}$ (purple solid) is indeed balanced by the sum of the field-particle energy transfer to ions and electrons (black dashed).

3.5. *Evolution of the Total Energy Budget*

Plots of the total energy budget as a function of time in the simulation nicely summarize the flow of energy in the simulation. First, we account for the energy lost from δW in

the `AstroGK` simulation to collisional plasma heating by accumulating the thermalized energy in each species over time, $E_s^{(coll)}(t) = \int_0^t dt' Q_S(t')$.

In Fig. 6(a), we plot the evolution of the energy budget over the course of the simulation, showing that turbulent energy $E^{(turb)}$, which dominates at the beginning of the simulation, is largely converted to ion heat $E_i^{(coll)}$ and electron heat $E_e^{(coll)}$ by the end of the simulation, with a smaller fraction of the lost turbulent energy persisting as non-thermal ion energy $E_i^{(nt)}$ and electron energy $E_e^{(nt)}$. Also indicated in Fig. 6(a) is the evolution of the total fluctuating energy δW (thick black line), showing that 60% of this energy has been lost to plasma heating over 7.5 periods of the initial Alfvén waves. Another interesting point is that, although electrons are heated twice as much as ions, the non-thermal electron energy content of the simulation always remains very small. This point is consistent with the idea, introduced in §3.4 above, that non-thermal energy transferred into the electron velocity distribution function by collisionless damping of the turbulence is very rapidly thermalized into electron heat. This analysis of the evolution of the total energy budget shows that energy is conserved to within 0.1% over the course of the simulation.

One can alternatively divide the contributions to the energy budget in terms of (3.1), as shown in Fig. 6(b), showing the perpendicular magnetic field energy $E_{B_\perp}$ (green), the parallel magnetic field energy $E_{B_\parallel}$ (cyan), the total fluctuating ion kinetic energy $E_i^{(\delta f)}$ (red), and the total fluctuating electron kinetic energy $E_e^{(\delta f)}$ (blue). Note that, as anticipated from the contributions to the turbulent energy in Fig. 2(b), the turbulent energy in Fig. 6(a) is largely composed of perpendicular magnetic energy $E_{B_\perp}$ and kinetic energy of the perpendicular ion bulk flows $E_{i,u_\perp}$. The wiggly boundary between $E_{B_\perp}$ and $E_{i,u_\perp}$ is a consequence of the Alfvénic fluctuations, and their nonlinear interactions, in the simulation.

One final point is that, although one may choose to decompose the different contributions to the energy using (3.1) in Fig. 6(b), by organizing the energies instead according to the turbulent energy $E^{(turb)} = \int d^3\mathbf{r}[(|\delta\mathbf{B}|^2 + |\delta\mathbf{E}|^2)/8\pi + \sum_s \frac{1}{2} n_{0s} m_s |\delta\mathbf{u_s}|^2]$ and the species non-thermal energies $E_s^{(nt)}$, the interpretation of the energy flow is much more physically motivated, as illustrated by Fig. 4. By simply plotting $E_i^{(\delta f)}$ as a function of time, one does not see the important split between the large fraction of the total fluctuating ion kinetic energy $E_i^{(\delta f)}$ that is associated with turbulent fluctuations and the remainder that corresponds to non-thermal energy not associated with turbulent fluctuations.

4. Development of Current Sheets and Intermittent Particle Energization

In the limit of strong nonlinearity, $\chi \sim 1$—corresponding to the important case of critically balanced, strong MHD turbulence (Goldreich & Sridhar 1995)—recent work has shown that Alfvén wave collisions self-consistently develop intermittent current sheets (Howes 2016). This finding may indeed explain the ubiquitous current sheets found to develop in simulations of plasma turbulence (Wan *et al.* 2012; Karimabadi *et al.* 2013; TenBarge & Howes 2013; Wu *et al.* 2013; Zhdankin *et al.* 2013) and inferred from spacecraft observations of the solar wind (Osman *et al.* 2011; Borovsky & Denton 2011; Osman *et al.* 2012; Perri *et al.* 2012; Wang *et al.* 2013; Wu *et al.* 2013; Osman *et al.* 2014). Yet how this self-consistent development of current sheets influences the physical mechanisms that remove energy from plasma turbulence remains unanswered. We show in this section that

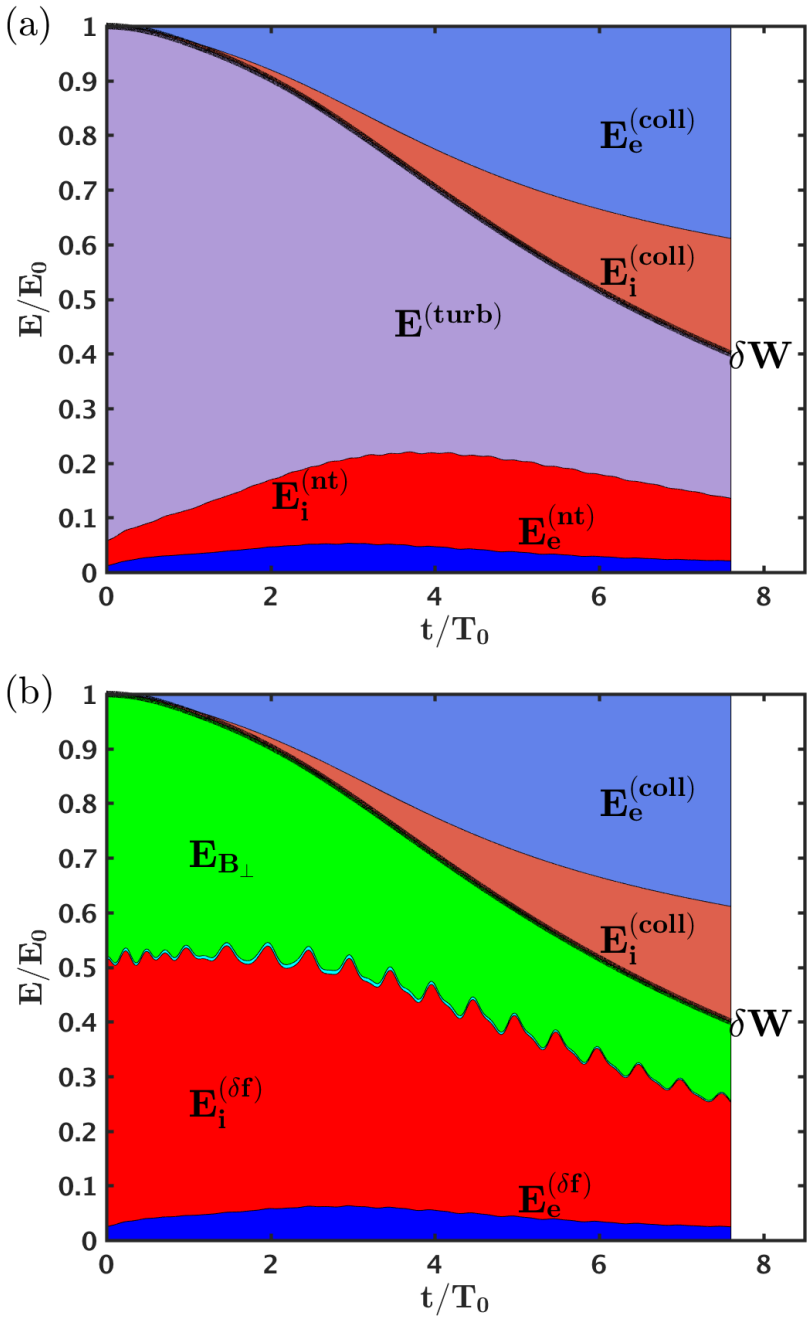


FIGURE 6. (a) The energy budget of the simulation vs. time, showing the turbulent energy $E^{(turb)}$, non-thermal ion energy $E_i^{(nt)}$, non-thermal electron energy $E_e^{(nt)}$, ion heat $E_i^{(coll)}$ and electron heat $E_e^{(coll)}$. (b) The same energy budget decomposed according to (3.1), showing the perpendicular magnetic field energy $E_{B_\perp}$, parallel magnetic field energy $E_{B_\parallel}$ (cyan, not labeled, appearing between $E_{B_\perp}$ and $E_i^{(\delta f)}$,), total fluctuating ion kinetic energy $E_i^{(\delta f)}$, total fluctuating electron kinetic energy $E_e^{(\delta f)}$, ion heat $E_i^{(coll)}$ and electron heat $E_e^{(coll)}$. The total fluctuating energy δW is shown in both panels (thick black line).

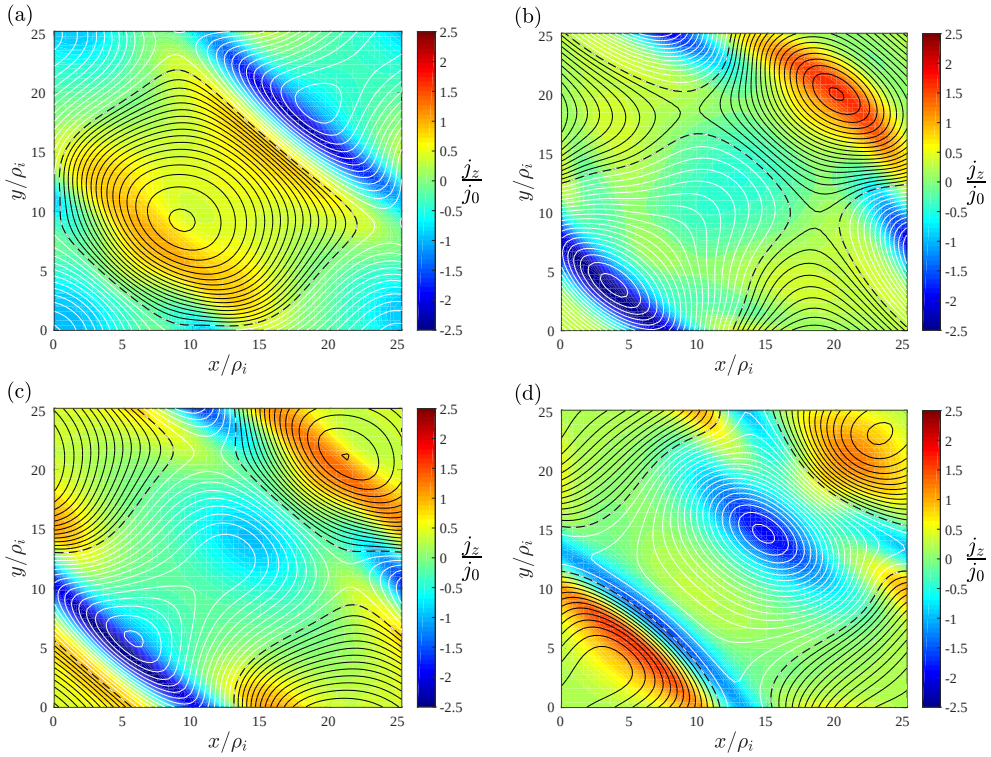


FIGURE 7. Plots of parallel current $j_\parallel/j_0$ (colorbar) and contours of the parallel vector potential $A_\parallel$ (contours, positive black, negative white) at times $t/T_0 =$ (a) 1.38, (b) 1.75, (c) 1.86, and (d) 2.03.

the simulation reported here indeed develops intermittent currents sheets (intermittent in both time and space), and in section §5 we employ the field-particle correlation technique to examine the physical mechanism that removes energy from the turbulent fluctuations.

In Fig. 7 we plot the current density parallel to the mean magnetic field $j_\parallel/j_0$ (colorbar) and contours of parallel vector potential $A_\parallel$ (positive black, negative white) in the plane $z/L_\parallel = -0.25$, where the simulation domain spans $-L_\parallel/2 \leqslant z \leqslant L_\parallel/2$ and $j_0 = n_0 q_i v_{ti} L_\perp / L_\parallel$. We plot evolution of the current in this plane at four different times in the evolution of the strong Alfvén wave collision, $t/T_0 =$ (a) 1.38, (b) 1.62, (c) 1.86, and (d) 2.10. Here $T_0 = 2\pi/\omega$ is the period of the initial Alfvén waves, where the gyrokinetic linear dispersion relation gives $\omega/k_\parallel v_A = 0.995$ and $\gamma/k_\parallel v_A = -6.10 \times 10^{-3}$. These plots show the presence of intermittent, elongated sheets of localized current density. Over a single initial Alfvén wave period T_0, two current sheets form at slightly different times, become thinner and more intense, and then disappear. One of these current sheets appears in the upper right quadrant of the plane $z/L_\parallel = -0.25$, and the other in the lower left quadrant, as shown in Fig. 7. During this time, their cross sections in the plane plotted in Fig. 7 moves slowly across the quadrant of the domain in which each appears (but these intermittent current sheets do not cross the entire domain, as would be expected from a strictly linear fluctuation). The general picture of current sheet development and evolution in a strong Alfvén wave collision is described in more quantitative detail by Howes (2016); although the parameters of this simulation are slightly different, the evolution of the current sheets is qualitatively similar here.

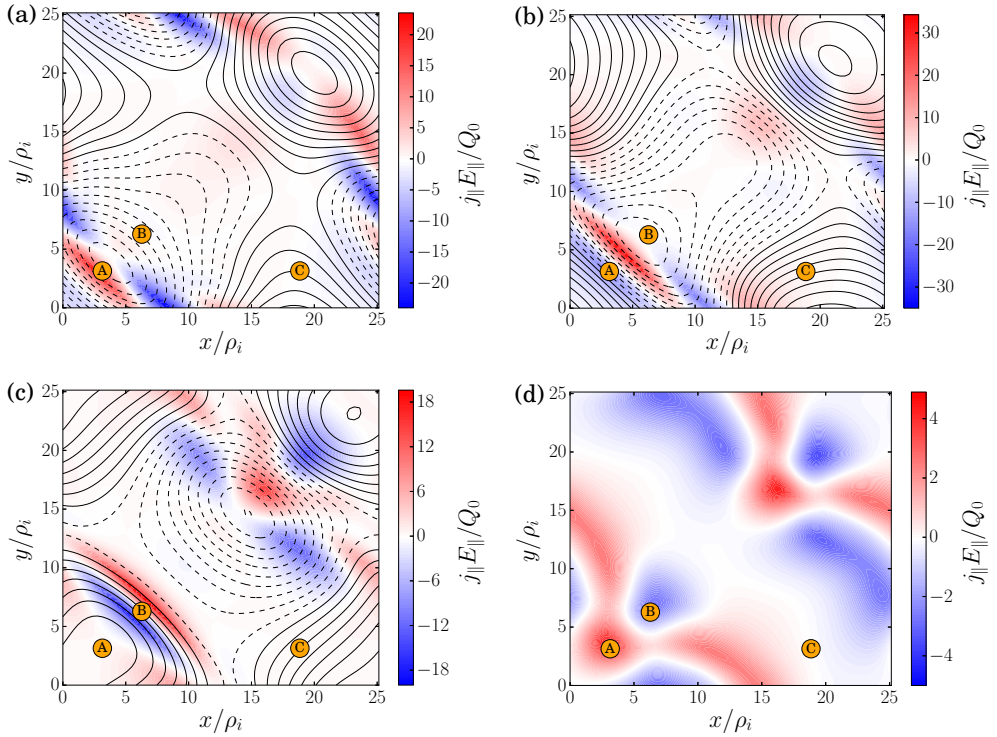


FIGURE 8. Plots of $j_\parallel E_\parallel$ (colorbar) and contours of the parallel vector potential $A_\parallel$ (contours, positive solid, negative dashed) at times $t/T_0 =$ (a) 1.75, (b) 1.86, and (c) 2.03, as well as (d) $\langle j_\parallel E_\parallel \rangle_\tau$, the rate of electromagnetic work per unit volume averaged over approximately one full wave period, $\tau = 0.992 T_0$, centered at time $t/T_0 = 1.86$.

4.1. *Spatial Distribution of Parallel Electromagnetic Work, $j_\parallel E_\parallel$*

As shown in §3, over the full time of the simulation, $7.5T_0$, 60% of the fluctuating energy δW of the initial Alfvén waves is removed from the fluctuations in the plasma. Fig. 3 shows that this energy is ultimately irreversibly converted into electron and ion heat through the weak but finite collisionality in the plasma. As the model of energy flow illustrated in Fig. 4 shows, this energy is initially removed from the turbulent electromagnetic fluctuations (Howes 2015, 2017) through collisionless interactions between the electromagnetic fields and the individual plasma particles. In a kinetic plasma, the rate of electromagnetic work done on the particles by the fields is given by $dW/dt = \int d^3\mathbf{r}\, \mathbf{j} \cdot \mathbf{E}$ (Howes *et al.* 2017; Klein 2017). Therefore, plotting the rate of electromagnetic work $\mathbf{j} \cdot \mathbf{E}$ as a function of position provides useful insights into the particle energization in the plasma.

As shown in Appendix B, in this simulation the dominant electromagnetic work is done by the component of the electric field parallel to the magnetic field, $E_\parallel$, so in Fig. 8 we plot the instantaneous value of dimensionless rate of work per unit volume $j_\parallel E_\parallel / Q_0$ as a function of position in the plane $z/L_\parallel = -0.25$ at three different times during the simulation $t/T_0 =$ (a) 1.75, (b) 1.86, and (c) 2.03. Note that the value of $j_\parallel E_\parallel$ is physically interpreted as the rate of transfer of spatial energy density between the parallel electric field $E_\parallel$ and the plasma ions and electrons. Since this electromagnetic work is reversible, its value can be positive or negative, where positive means work done on the particles by the field, and negative means work done on the field by the particles.

As emphasized in Howes *et al.* (2017), the instantaneous energy transfer between fields and particles has two components: (i) an *oscillating energy transfer* back and forth between fields and particles that is typical of undamped linear wave motion in a kinetic plasma, and (ii) a *secular energy transfer* that represents the energy lost from the electromagnetic fluctuations to the plasma particles through collisionless damping. To determine the particle energization, it is the secular energy transfer that is of interest, but the challenge is that the oscillating energy transfer often has a much larger amplitude than the secular energy transfer. However, if a time-average is taken over a suitably chosen averaging interval, the oscillating energy transfer will largely cancel out, exposing the smaller secular energy transfer that is sought. In this strong Alfvén wave collision simulation, the linear period T_0 of the initial Alfvén waves is an appropriate choice for this time-averaging, and we plot in Fig. 8(d) the time-average of $\langle j_\parallel E_\parallel \rangle_\tau$ over an interval $\tau = 0.992 T_0$ centered at time $t/T_0 = 1.86$.

The plots shown in Fig. 8 convey a number of valuable insights into the particle energization in this simulation. First, the plots in Fig. 8(a)-(c) show clearly that the instantaneous rate of energy transfer is both spatially and temporally intermittent, with the energy transfer localized in sheet-like structures reminiscent of the current sheets plotted in Fig. 7. An example of the temporal variation is illustrated by observing the changes in the instantaneous energy transfer rate at point A marked on each plot. At (a) $t/T_0 = 1.75$, the plasma is energized by $E_\parallel$, but later at (b) $t/T_0 = 1.86$ the plasma is losing energy to $E_\parallel$, and finally at (c) $t/T_0 = 2.03$ there is very little energy transfer either direction. Averaged over one period, Fig. 8(d) shows that the plasma gains energy from the parallel electric field at point A. Curiously, the instantaneous energy transfer from fields to particles at $t/T_0 = 1.86$ in Fig. 8(b) is negative at point A, but the single-period average, centered at that same time $t/T_0 = 1.86$ in Fig. 8(d) shows a positive transfer of energy to the particles at the same position. This plot stresses the importance of appropriate time-averaging to properly understand the net particle energization in a turbulent plasma.

Second, the net plasma energization over one period in Fig. 8(d) is also spatially intermittent, with plasma energization at point A, a net loss of energy at point B, and little energy change at point C. It is also worthwhile pointing out that the magnitude of the time-averaged energy transfer is smaller in magnitude than the instantaneous energy transfer, as expected if some fraction of this energy transfer is oscillatory and largely cancels out when averaged over one period T_0. Together, the four panels demonstrate the key point that that the particle energization is spatially non-uniform, both instantaneously as well as when averaged over one period T_0 of the initial Alfvén waves.

Third, something that cannot be appreciated by the single time slice in Fig. 8(d), is the surprising result that the single-period-averaged plasma energization has very little temporal variation as the center of the time-average window is advanced over one period. In fact, one observes only a very slow evolution of this particle energization pattern over a number of periods, probably due to the long-term evolution and accumulating loss of fluctuating energy δW over the course of the simulation.

A final point is that the plasma energization—the sum of the energy transfer to both ions and electrons—has a net positive value when integrated over the entire simulation domain, as demonstrated by the sum $\dot{E}_i^{(fp)} + \dot{E}_e^{(fp)}$ plotted in Fig. 5(c). Therefore, although there is a loss of plasma energy in some regions of the domain, the net effect is that plasma species gain energy at the expense of the turbulent electromagnetic field and bulk plasma flow fluctuations, as depicted in the energy flow diagram in Fig. 4.

Further insight into the effect of the nonlinear evolution on the resulting plasma en-

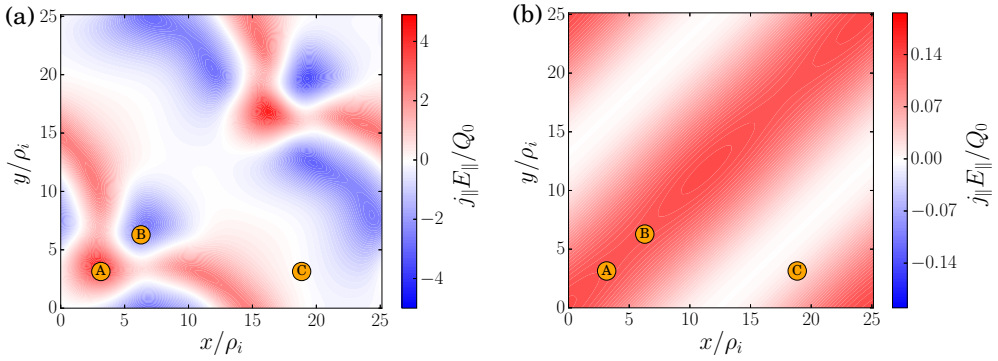


FIGURE 9. Comparison of time-averaged $\langle j_\parallel E_\parallel \rangle_\tau$ over an interval $\tau = 0.992T_0$ centered at time $t/T_0 = 1.86$ for both (a) a nonlinear run and (b) a linear run, starting from identical initial conditions, showing a much more spatially intermittent distribution of plasma energization in the nonlinear case.

ergization can be gained by comparing a linear simulation starting from identical initial conditions. In the linear case, no energy is transferred to other Fourier modes, and all of the particle energization is due to linear collisionless damping via the Landau resonance. In Fig. 9, we plot the time-averaged $\langle j_\parallel E_\parallel \rangle_\tau$ over an interval $\tau = 0.992T_0$ centered at time $t/T_0 = 1.86$ for both (a) the nonlinear run and (b) the linear run. This figure directly demonstrates the striking fact that the spatial non-uniformity of particle energization arises due to the nonlinear transfer of energy to other Fourier modes. This is fully consistent with the picture of current sheet generation by constructive interference among the initial Alfvén wave modes and the nonlinearly generated fluctuations (Howes 2016). In §5, the field-particle correlation technique will be used to identify the nature of the collisionless energy transfer that yields this spatially non-uniform particle energization.

The rate of plasma energization is the sum of the rates of ion and electron energization, $j_\parallel E_\parallel = j_{\parallel i} E_\parallel + j_{\parallel e} E_\parallel$, and, in Appendix B, we plot in Figs. 16 and 17 the separate ion and electron energization contributing to Fig. 8. In this simulation, the single-period averaged particle energization in the plane $z/L_\parallel = -0.25$ shown in Fig. 8 yield about twice the energy transfer to electrons relative to the ions at $t/T_0 = 1.86$.

5. Analysis of Energy Transfer Mechanism Using Field-Particle Correlations

The rates of total energy transfer as a function of time between the turbulent fluctuations and the ions and electrons, plotted in Fig. 5, give the desired information about the net collisionless particle energization over the entire simulation domain. But this simple approach cannot be applied to the analysis of spacecraft measurements to understand heating in heliospheric plasmas, because spacecraft measure the particle velocity distributions and electromagnetic fields at only one or a few points in space, so it is not possible to integrate the plasma heating over the entire plasma volume. In addition, such an energy flow analysis alone, such as that given in the diagram in Fig. 4, tells us nothing of the mechanism leading to the particle energization.

The electromagnetic work, $\mathbf{j} \cdot \mathbf{E}$, can be computed with single point measurements, providing more insight into the nature of the particle energization mechanism and the spatial distribution of energy transfer than an energy analysis alone, but the newly developed field-particle correlation technique (Klein & Howes 2016; Howes *et al.* 2017), which yields

the distribution of the energy transfer as a function of particle velocity, gives far greater detail about the nature of the energy transfer mechanism. This technique requires only a single-point time series of both field and velocity distribution function measurements, which can be obtained using modern spacecraft instrumentation.

The field-particle correlation technique has been successfully applied to examine the electron energization due to the damping of electrostatic fluctuations in a 1D-1V Vlasov-Poisson plasma (Klein & Howes 2016; Howes *et al.* 2017), to determine the transfer of free energy in kinetic instabilities from unstable particle velocity distributions to electrostatic fluctuations (Klein 2017), and to explore the particle energization caused by the collisionless damping of strong, broadband, gyrokinetic plasma turbulence (Klein *et al.* 2017). Here we apply the technique to discover the nature of the physical mechanism responsible for the spatially intermittent transfer of energy from the turbulent fluctuations to the non-thermal energy of the ions and electrons in the plasma.

Specifically, since we know from Fig. 15 in Appendix B that the net energy transfer is dominated by the parallel electric field, we will evaluate the correlation of the ion and electron fluctuations with the parallel electric field. The correlation of the parallel electric field, $E_\parallel$, with a species s is defined by

$$C_{E_\parallel,s}(\mathbf{v},t,\tau) = C\left(-q_s\frac{v_\parallel^2}{2}\frac{\partial f_s(\mathbf{r}_0,\mathbf{v},t)}{\partial v_\parallel}, E_\parallel(\mathbf{r}_0,t)\right). \tag{5.1}$$

This unnormalized correlation is taken over an appropriately chosen correlation interval τ to suppress the signal of the oscillatory energy transfer relative to the secular energy transfer (Howes *et al.* 2017). Defining the *phase-space energy density* by $w_s(\mathbf{r},\mathbf{v},t) = m_s v^2 f_s(\mathbf{r},\mathbf{v},t)/2$, this unnormalized correlation yields the phase-space energy transfer rate between the parallel electric field $E_\parallel$ and species s given by the Lorentz term in the Vlasov equation (Howes 2017; Klein *et al.* 2017). A key aspect of this novel analysis method is that it retains the dependence of the energy transfer on velocity space. Note that integrating this correlation over velocity space simply yields the parallel contribution to the electromagnetic work, $j_\parallel E_\parallel = \int d\mathbf{v} C_{E_\parallel}(\mathbf{v},t,\tau)$ (Howes *et al.* 2017; Klein *et al.* 2017).

For the application of this technique to data from our gyrokinetic simulation using `AstroGK`, we note that the gyrokinetic distribution function $h_s(x,y,z,v_\perp,v_\parallel)$ is related to the total distribution function f_s via (Howes *et al.* 2006)

$$f_s(\mathbf{r},\mathbf{v},t) = F_{0s}(v)\left(1-\frac{q_s\phi(\mathbf{r},t)}{T_{0s}}\right) + h_s(\mathbf{r},v_\parallel,v_\perp,t). \tag{5.2}$$

As a technical step, we transform from the gyrokinetic distribution function h_s to the complementary perturbed distribution function

$$g_s(\mathbf{r},v_\parallel,v_\perp) = h_s(\mathbf{r},v_\parallel,v_\perp) - \frac{q_s F_{0s}}{T_{0s}}\left\langle \phi - \frac{\mathbf{v}_\perp\cdot\mathbf{A}_\perp}{c}\right\rangle_{\mathbf{R}_s}, \tag{5.3}$$

where $\langle ... \rangle$ is the gyroaveraging operator (Schekochihin *et al.* 2009). The complementary distribution function g_s describes perturbations to the background distribution in the frame of reference moving with the transverse oscillations of an Alfvén wave. Field-particle correlations calculated using h_s or f_s yield qualitatively and quantitatively similar results to those computed with g_s (Klein *et al.* 2017).

Below, we present the correlations between the complementary perturbed distribution

function and the parallel electric field $E_\parallel$ at a single-point $\mathbf{r}_0$

$$C_{E_\parallel,s}(v_\parallel, v_\perp, t, \tau) = C\left(-q_s \frac{v_\parallel^2}{2} \frac{\partial g_s(\mathbf{r}_0, v_\parallel, v_\perp, t)}{\partial v_\parallel}, E_\parallel(\mathbf{r}_0, t)\right). \tag{5.4}$$

To explore the particle energization over time, we can also integrate over the perpendicular velocity $v_\perp$ to obtain a reduced parallel correlation

$$C_{E_\parallel,s}(v_\parallel, t, \tau) = \int v_\perp dv_\perp C_{E_\parallel,s}(v_\parallel, v_\perp, t, \tau). \tag{5.5}$$

This reduced parallel correlation $C_{E_\parallel,s}(v_\parallel, t, \tau)$ can be plotted as a function of $(v_\parallel, t)$ to illustrate the time evolution particle energization using a timestack plot of the energy transfer as a function of the parallel velocity of the particles.

5.1. *Timestack Plots of Field-Particle Correlations*

Here we present the results of the field-particle technique applied at three points in the simulation domain, labeled A, B, and C in Fig. 8. From Fig. 8(d), we see that, averaged over one period $\tau/T_0 = 0.992$ centered at $t/T_0 = 1.86$, there is a net gain of energy by the plasma at point A, a net loss of energy by the plasma at point B, and little net change in the plasma energy at point C. Note that the reduced parallel correlation $C_{E_\parallel,s}(v_\parallel, t, \tau)$ in the plots presented in this section is normalized by the energy transfer rate per unit volume per unit velocity, Q_0/v_{ti}.

In Fig. 10(b), we present a timestack plot of the reduced parallel field-particle correlation for the ions $C_{E_\parallel,i}(v_\parallel, t, \tau)$ at position A with a correlation interval $\tau/T_0 = 0.992$, showing the distribution of the energy transfer to the ions as a function of the parallel velocity $v_\parallel/v_{ti}$ vs. normalized time t/T_0. Vertical solid and dashed black lines indicate the limits of resonant parallel phase velocities from Fig. 1, $1.0 \lesssim |\omega/k_\parallel v_{ti}| \lesssim 1.5$ for ions; there are both positive and negative ranges of parallel phase velocities, corresponding to Alfvén waves traveling up or down the mean magnetic field. Also plotted in Fig. 10(a) is the velocity-space integrated correlation, $\partial w_i/\partial t = \int dv_\parallel C_{E_\parallel i}(v_\parallel, t, \tau)$, equivalent to the parallel ion contribution of the electromagnetic work $j_{\parallel i}E_\parallel$ at position A, showing a net energization of the ions over the course of the simulation.

The distribution of the energy transfer as a function of $v_\parallel/v_{ti}$ in Fig. 10(b) is the *velocity space signature* of the energy transfer mechanism. The localization of the energy transfer in the marked range of resonant parallel phase velocities for kinetic Alfvén waves clearly indicates that the energy transfer is resonant. The specific distribution of this energy transfer, with a transfer of energy from $E_\parallel$ to the ions (red) at $|v_\parallel/v_{ti}| > |v_{res}/v_{ti}|$ and a loss of energy from the ions (blue) at $|v_\parallel/v_{ti}| < |v_{res}/v_{ti}|$ is the characteristic signature of the Landau damping of kinetic Alfvén waves (Howes 2017; Klein *et al.* 2017). The change of sign in the energy transfer occurs at the resonant phase velocity for the collisionlessly damped wave. Here the change of sign occurs at $v_\parallel/v_{ti} = \omega/k_\parallel v_{ti} \simeq v_A/v_{ti} = \pm 1$, indicating that larger scale Alfvén waves with $k_\perp \rho_i \ll 1$, which have a parallel phase velocity $\omega/k_\parallel = v_A$, appear to dominate the energy transfer at point A. This is consistent with the fact the energy in the electromagnetic and plasma bulk flow fluctuations in this simulation is dominated by the low $k_\perp \rho_i \ll 1$ modes. This novel field-particle correlation analysis shows definitively the key result that ion Landau damping contributes to the energization of ions at position A in this strong Alfvén wave collision simulation.

In Fig. 10(d), we plot the the reduced parallel field-particle correlation for the electrons $C_{E_\parallel,e}(v_\parallel, t, \tau)$ at position A with the same correlation interval $\tau/T_0 = 0.992$, where vertical solid and dashed black lines indicate the range of resonant parallel velocities from

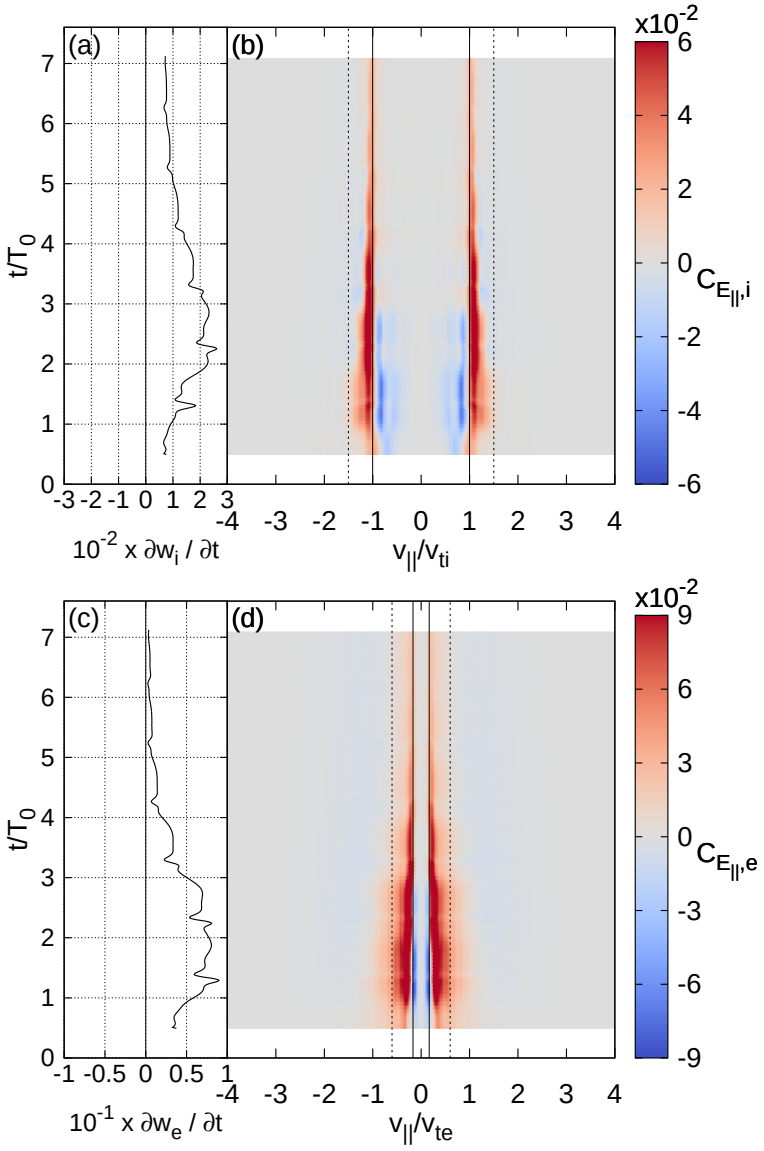


FIGURE 10. Timestack plots of ion and electron energization at position A for a correlation interval $\tau/T_0 = 0.992$. (a) Velocity-space integrated correlation, giving the rate of ion energization $\partial w_i/\partial t$ due to ion interactions with $E_\parallel$. (b) The reduced parallel field-particle correlation for the ions $C_{E_\parallel,i}(v_\parallel, t, \tau)$. (c) Velocity-space integrated correlation, giving the rate of electron energization $\partial w_e/\partial t$ due to electron interactions with $E_\parallel$.(d) The reduced parallel field-particle correlation for the electrons $C_{E_\parallel,e}(v_\parallel, t, \tau)$. Vertical solid black indicate resonant velocities for a parallel phase velocity at the Alfvén speed $\omega/(k_\parallel v_{ts}) = v_A/v_{ts}$. Vertical dashed lines indicate the highest parallel phase velocities for modes with significant collisionless damping in the simulation.

Fig. 1, $0.17 \lesssim \omega/k_\parallel v_{te} \lesssim 0.6$ for electrons. Also plotted in Fig. 10(c) is the the velocity-space integrated correlation, $\partial w_e/\partial t = \int dv_\parallel C_{E_\parallel e}(v_\parallel, t, \tau)$, equivalent to the parallel electron contribution of the electromagnetic work $j_{\parallel e}E_\parallel$, showing a net energization of the electrons at position A.

The velocity space signature of the electron energization in Fig. 10(d) also shows the typical characteristics of electron Landau damping, with a slight difference from the ion case. Because kinetic Alfvén waves are dispersive, with a parallel phase velocity that increases for $k_\perp \rho_i \gtrsim 1$ given approximately by $\omega = k_\parallel v_A \sqrt{1 + (k_\perp \rho_i)^2/[\beta_i + 2/(1 + T_e/T_i)]}$ (Howes *et al.* 2014), the parallel resonant velocity will increase for kinetic Alfvén waves with larger $k_\perp \rho_i$. The velocity space signature of linear Landau damping typically shows the change of sign of the energy transfer at the resonant velocity. In Fig. 10(d), that change of sign for $1 \leqslant t/T_0 \leqslant 3$ occurs at a resonant velocity slightly larger than v_A/v_{te} (vertical black line), suggesting that the kinetic Alfvén wave involved in the electron Landau damping has a value of $k_\perp \rho_i \gtrsim 1$ leading to a higher resonant parallel velocity. Despite this minor detail, the energy transfer still shows that the electron energization is mediated by resonant electrons, with a velocity space signature typical of electron Landau damping (Howes 2017). Therefore, this analysis definitively yields a second key result, that electron Landau damping contributes to the energization of electrons at position A in this strong Alfvén wave collision simulation.

We can also investigate the regions in the simulation domain where the plasma loses energy to the parallel electric field at point B, plotted in Fig. 11. The (a) velocity-integrated ion energization $\partial w_i/\partial t$ due to $E_\parallel$ and (c) velocity-integrated electron energization $\partial w_e/\partial t$ due to $E_\parallel$ both show that the net energy transfer to ions and electrons at point B is negative. Here, as in Fig. 10, we see that the energy transfer for both ions in panel (b) and electrons in panel (d) is dominated by particles with velocities that fall within the range of parallel velocities expected to be resonant with the parallel phase velocity of Alfvén waves, demonstrating directly that energy transfer between the particles and the parallel electric field $E_\parallel$ is governed by Landau resonant interactions.

At point C in the simulation domain, there is very little net energy transfer from the parallel electric field to the plasma particles. The same field-particle correlation analysis at point C, presented in Fig. 12, shows that the velocity-integrated (a) ion energization $\partial w_i/\partial t$ and (c) electron energization $\partial w_e/\partial t$ due to $E_\parallel$ yields a very small positive transfer of energy to the particles over the first couple of periods T_0, with an amplitude about an order of magnitude smaller than the energy transfer at points A and B. The reduced parallel field-particle correlation $C_{E_\parallel,s}(v_\parallel, t, \tau)$ for (b) the ions and (d) the electrons shows that the majority of this very small amount of energy transfer is still dominated by resonant particles.

But there is a very significant difference between the reduced parallel field-particle correlation $C_{E_\parallel,s}$ at point C for both ions and electrons compared to the same correlation at points A and B: the pattern of energy transfer at point C is dominantly odd in $v_\parallel$, whereas the patterns at points A and B are dominantly even in $v_\parallel$. When integrated over the parallel velocity to obtain the net change of energy of a species, an odd pattern largely cancels out, whereas an even pattern does not. Therefore, there is little net particle energization at point C, even though individual particles do gain and lose energy through resonant interactions with $E_\parallel$. Particles with $v_\parallel > 0$ gain nearly the same amount of energy as that lost by particles with $v_\parallel < 0$, yielding little net change of particle energy.

The important point that the field-particle correlation analysis here demonstrates is that collisionless interactions of the Landau resonance between $E_\parallel$ and the ions and electrons contribute to the spatially intermittent pattern of time-averaged particle energization, shown in Fig. 8(d). This result disproves by counterexample the commonly stated belief that Landau damping can only lead to spatially uniform particle energization. Rather, we see clearly here that collisionless damping via the Landau resonance can indeed be responsible for spatially localized particle energization, as previously suggested in the literature (TenBarge & Howes 2013; Howes 2015, 2016). Furthermore, the nonlin-

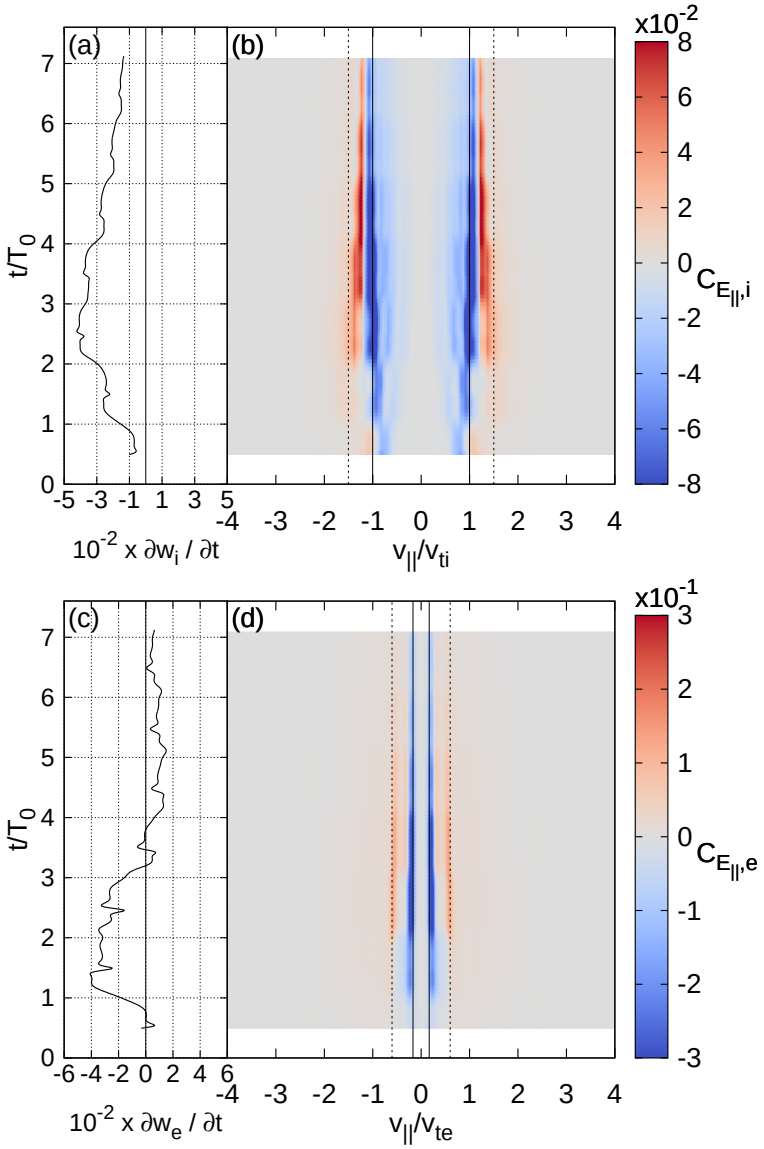


FIGURE 11. Plots of the same field-particle correlation analysis as Fig. 10, but taken at point B.

ear energy transfer by collisionless damping via the Landau resonance is not inhibited by the strong nonlinear interactions that play an important role in this strong Alfvén wave collision simulation. Indeed, nonlinear gyrokinetic simulations of strong, broadband plasma turbulence have indeed shown that the collisionless transfer of energy between fields and ions is dominated by particles approximately in Landau resonance with the parallel phase velocity of Alfvénic fluctuations (Klein *et al.* 2017).

5.2. *Particle Energization in Gyrotropic Velocity Space*

Finally, we can examine the distribution of particle energization in gyrotropic velocity space $(v_\parallel, v_\perp)$ (Howes 2017) using the field-particle correlation $C_{E_\parallel,s}(v_\parallel, v_\perp, t, \tau)$. Although plots of this analysis are limited to the correlation centered at just a single point

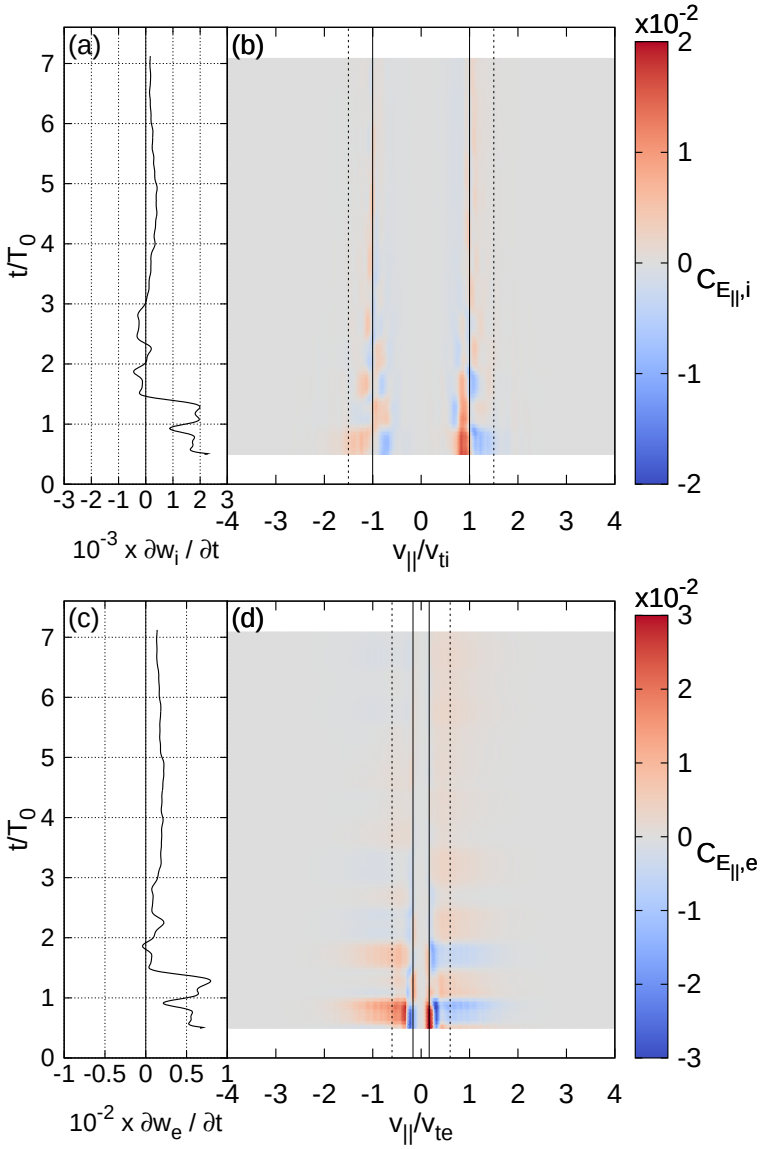


FIGURE 12. Plots of the same field-particle correlation analysis as Fig. 10, but taken at point C.

in time, by not integrating over perpendicular velocity $v_\perp$ one obtains complete information about which particles in gyrotropic velocity space $(v_\parallel, v_\perp)$ participate in the collisionless transfer of energy. Note that the parallel correlation in gyrotropic velcotiy space, $C_{E_\parallel,s}(v_\parallel, v_\perp, t, \tau)$ in the plots presented in this section is normalized by the energy transfer rate per unit volume per unit velocity squared, Q_0/v_{ti}^2.

In Fig. 13, we plot $C_{E_\parallel,s}(v_\parallel, v_\perp, t, \tau)$ for the same correlation interval $\tau/T_0 = 0.992$ centered at time $t/T_0 = 2.10$: (a) ion and (b) electron energization at point A, (c) ion and (d) electron energization at point B, and (e) ion and (f) electron energization at point C. As before, vertical solid and dashed black lines denote the range of resonant parallel velocities for Alfvén waves. Three important points can be inferred from these

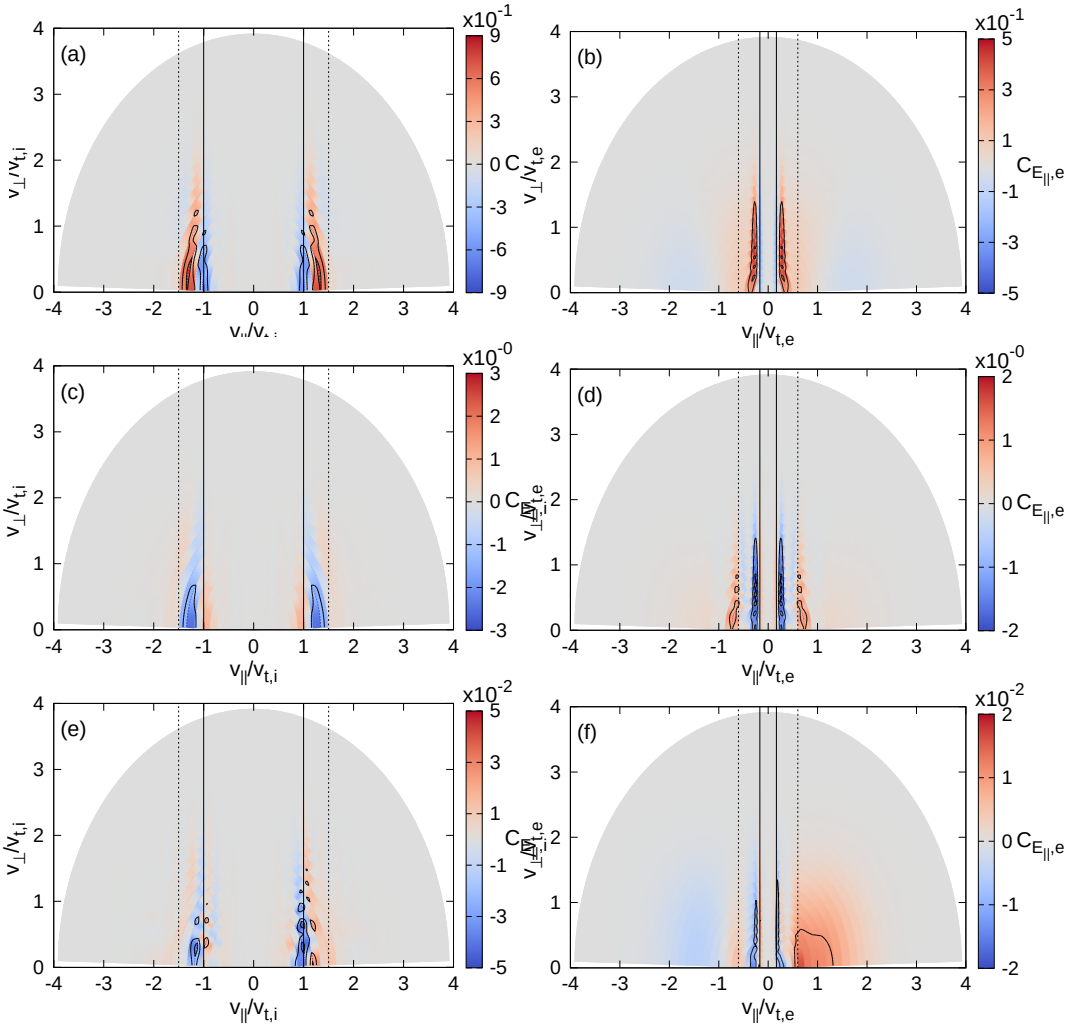


FIGURE 13. Plots of the field-particle correlation $C_{E_\parallel}(v_\parallel, v_\perp, t, \tau)$ on gyrotropic velocity space $(v_\parallel, v_\perp)$ for a correlation interval $\tau/T_0 = 0.992$ centered at time $t/T_0 = 2.10$: (a) ion and (b) electron energization at point A, (c) ion and (d) electron energization at point B, and (e) ion and (f) electron energization at point C. Vertical solid lines denote the resonant parallel velocities for a parallel phase velocity at the Alfvén speed $\omega/(k_\parallel v_{ts}) = v_A/v_{ts}$.

gyrotropic velocity space plots. First, other than a steady decrease of the amplitude of the signal with increasing $v_\perp$—as expected because the equilibrium Maxwellian distribution drops off exponentially as $\exp(-v^2/v_{ts}^2)$, so the amplitude of fluctuations $\delta f(\mathbf{v})$ would be expected to have a similar drop off in amplitude—the energy transfer shows very little variation with $v_\perp$. The variation in the energy transfer is organized almost entirely by $v_\parallel$, as expected for a Landau resonant energy transfer process. Second, this energy transfer is dominated by particles with parallel velocities resonant with Alfvénic fluctuations, $v_\parallel \simeq v_A$, demonstrating that the energy transfer is governed by the Landau resonance. Third, the odd or even character in $v_\parallel$ at the different points A, B, and C seen in the timestack plots is also clearly apparent here in these gyrotropic velocity space plots.

Summarizing, the gyrotropic velocity space $(v_\parallel, v_\perp)$ plots in Fig. 13 demonstrate how the field-particle correlation technique maximizes the use of the full particle velocity

distribution function information, enabling the physical mechanism responsible for the removal of energy from turbulent fluctuations and consequent particle energization to be identified definitively. In this case, the velocity-space signature of the field-particle correlation is unmistakably that of Landau damping of a kinetic Alfvén wave (Howes 2017), proving that Landau damping indeed plays a role in the spatially intermittent removal of the energy of electromagnetic and bulk plasma flow fluctuations, even in the presence of strong nonlinearity.

6. Conclusion

Using a nonlinear gyrokinetic simulation of a strong Alfvén wave collision, we examine here the damping of the electromagnetic fluctuations and the associated energization of particles that occurs in current sheets that are generated self-consistently during the nonlinear evolution.

The flow of energy due to the collisionless damping and the associated particle energization, as well as the subsequent thermalization of the particle energy by collisions, provides an important framework for interpreting the nonlinear dynamics and dissipation. Fig. 4 presents a simple model of the energy flow from turbulent energy to plasma heat in the simulation, with the following two key stages: (i) the turbulent fluctuation energy is removed by collisionless field-particle interactions, transferring that energy reversibly into non-thermal energy of the plasma species; and (ii) the non-thermal energy, represented by fluctuations in the particle velocity distribution functions, is driven to sufficiently small velocity-space scales that weak collisions can thermalize that energy, irreversibly heating the plasma species. In the strong Alfvén wave collision simulated here, this two-step processes ultimately leads to more than 60% of the original fluctuation energy being dissipated collisionally as thermal ion and electron energy.

It has long been appreciated that the nonlinear evolution of plasma turbulence leads to the development of intermittent current sheets (Matthaeus & Montgomery 1980; Meneguzzi *et al.* 1981), and a recent study has shown that strong Alfvén wave collisions—nonlinear interactions between counterpropagating Alfvén waves—self-consistently develop intermittent current sheets through the constructive interference of the original Alfvén waves and nonlinearly generated fluctuations (Howes 2016). MHD turbulence simulations have shown that the dissipation of turbulent energy is largely concentrated in these intermittent current sheets (Uritsky *et al.* 2010; Osman *et al.* 2011; Zhdankin *et al.* 2013), so a natural question is whether the collisionless damping of current sheets generated by strong Alfvén wave collisions leads to such spatially intermittent particle energization. Plotting the spatial distribution of the electromagnetic work done by the parallel electric field $E_\parallel$, shown in Fig. 8(a)–(c), shows that the instantaneous particle energization is indeed spatially intermittent with a sheet-like morphology.

A key point, however, is that much of this reversible electromagnetic work leads to an oscillatory transfer of energy to and from the particles associated with undamped wave motion. Only by averaging over a suitable time interval, in this case an averaging interval that is approximately a single wave period $\tau \simeq T_0$, can we determine the secular particle energization $\langle j_\parallel E_\parallel \rangle_\tau$ associated with the net removal of energy from the turbulent fluctuations. Fig. 8(d) shows that the secular particle energization $\langle j_\parallel E_\parallel \rangle_\tau$ in this strong Alfvén wave collision indeed remains spatially intermittent, although less localized than the instantaneous rates of energy transfer in Fig. 8(a)–(c). The bottom line is that the current sheets arising in strong Alfvén wave collisions indeed generate spatially localized particle energization, consistent with that found in simulations of plasma turbulence (Wan *et al.* 2012; Karimabadi *et al.* 2013; TenBarge & Howes 2013; Wu *et al.* 2013; Zhdankin *et al.*

2013) and inferred from spacecraft observations of the solar wind (Osman *et al.* 2011, 2012; Perri *et al.* 2012; Wang *et al.* 2013; Wu *et al.* 2013; Osman *et al.* 2014).

The next obvious question is what is the physical mechanism governing the removal of energy from the turbulence and the consequent spatially intermittent energization of the particles? Using the recently developed field-particle correlation technique (Klein & Howes 2016; Howes *et al.* 2017), we examine how the energy transfer to ions and electrons by the parallel electric field $E_\parallel$ is distributed in velocity space. In other words, which particles in velocity space receive the energy transferred collisionlessly from the electromagnetic fields? The results, exemplified by Fig. 10, show that the particles that are resonant with the parallel velocity of the Alfvén waves in the simulation dominate the energy transfer, demonstrating conclusively that Landau damping plays a role in the damping of the electromagnetic fluctuations and consequent energization of the particles in this strongly nonlinear simulation.

Based on the plane-wave decomposition typically used to derive linear Landau damping analytically, one may naively expect that Landau damping leads to spatially uniform energization. Together, the results presented here definitively show instead that Landau damping can indeed lead to spatially intermittent particle energization. The comparison to a strictly linear simulation from identical initial conditions, presented in Fig. 9, shows that the nonlinear energy transfer to other Fourier modes is essential for the localization of the particle energization. This is consistent with the model for current sheet generation in Alfvén wave collisions in which nonlinearly generated modes constructively interfere with the initial Alfvén waves to create spatially intermittent current sheets; linear Landau damping of each of these modes, which occurs spatially locally, leads to the intermittent spatial pattern of the energization, as previously suggested (Howes 2015, 2016).

Our result here, that Landau damping is effective even in a plasma where strong nonlinear interactions are playing an important role, also addresses the important question of whether Landau damping is effective in a strongly turbulent plasma (Plunk 2013; Schekochihin *et al.* 2016). Our results here complement a recent field-particle correlation analysis of gyrokinetic turbulence simulations showing that Landau damping indeed persists as an effective physical mechanism for ion energization in broadband, strong plasma turbulence (Klein *et al.* 2017).

We emphasize here that we have not shown that Landau damping is the *only* damping mechanism, but we have provided conclusive evidence that Landau damping does play a role in the collisionless damping of turbulence in intermittent current sheets that arise from strong Alfvén wave collisions. As mentioned in Appendix B, transit-time damping (Barnes 1966; Quataert 1998)—which does work on particles via their magnetic moment through the magnetic mirror force arising from fluctuations in the magnetic field magnitude—is another effective physical mechanism for collisionless damping and energization of particles via the Landau resonance in gyrokinetics. Here we have focused only on the contribution to the particle energization by the parallel electric field $E_\parallel$; future work will address the additional contribution by the magnetic mirror force arising from $\nabla_\parallel |\mathbf{B}|$.

The comparison of the time evolution of the field-particle energy transfer $\dot{E}_s^{(fp)}$ and the collisional heating Q_s for each species in Fig. 5 also raises important questions about the relative rates of linear and nonlinear phase-mixing processes that enable the non-thermal energy, represented by fluctuations in the particle velocity distribution function, to reach sufficiently small velocity-space scales to be thermalized by arbitrarily weak collisions. These questions, and more, about the flow of energy in weakly collisional heliospheric

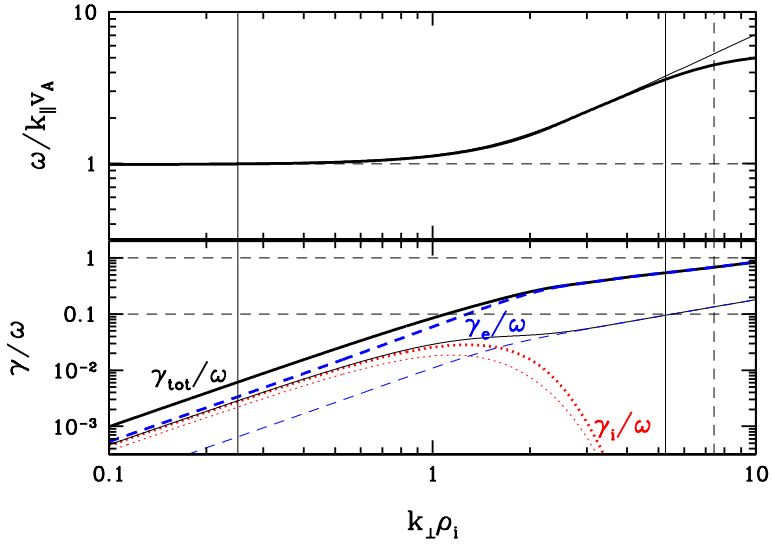


FIGURE 14. Comparison of the results from the linear collisionless gyrokinetic dispersion relation for the reduced mass ratio $m_i/m_e = 36$ (thick) and a realistic proton-to-electron mass ratio $m_i/m_e = 1836$ (thin): (a) normalized frequency $\omega/k_\parallel v_A$ and (b) total collisionless damping rate γ_{tot}/ω (black solid), ion collisionless damping rate γ_i/ω (red dotted), and electron collisionless damping rate γ_e/ω (blue dashed). Solid and dashed vertical lines are the same as in Fig. 1.

plasmas, lie at the forefront of kinetic heliophysics (Howes 2017), and will drive research efforts by the next generation of space plasma physicists.

This work was supported by NSF CAREER Award AGS-1054061, NASA HSR grant NNX16AM23G, DOE grant DE-SC0014599, and the University of Iowa Mathematical and Physical Sciences Funding Program. This work used the Extreme Science and Engineering Discovery Environment (XSEDE), which is supported by National Science Foundation grant number ACI-1053575, through NSF XSEDE Award PHY090084.

Appendix A. Collisionless Damping Rate as a Function of Mass Ratio

Here we present in Fig. 14 a comparison of the linear physics of the Alfvén/kinetic Alfvén wave mode for the reduced mass ratio used here $m_i/m_e = 36$ (thick lines) to that for a realistic proton-to-electron mass ratio $m_i/m_e = 1836$ (thin lines). Specifically, for a plasma with $\beta_i = 1$ and $T_i/T_e = 1$, we solve the linear collisionless gyrokinetic dispersion relation (Howes *et al.* 2006) for the (a) normalized wave frequency $\omega/k_\parallel v_A$ and (b) total collisionless damping rate γ_{tot}/ω (black solid) as a function of the perpendicular wavenumber $k_\perp \rho_i$. In addition, in panel (b) we also show the separate contributions of the ions (red dotted) and electrons (blue dashed) to the collisionless damping rate.

The comparison shows that the linear wave frequency $\omega/k_\parallel v_A$ begins to differ only slightly between the two cases at $k_\perp \rho_i \gtrsim 5$. Note that the fully resolved perpendicular range of the dealiased pseudospectral method for the strong Alfvén wave collision simulation covers $0.25 \leqslant k_\perp \rho_i \leqslant 5.25$, denoted by the two vertical solid black lines; modes in the corner of (k_x, k_y) Fourier space represent perpendicular wavenumbers out to $k_\perp \rho_i = 5.25\sqrt{2} \simeq 7.42$, denoted by the vertical dashed black line. Therefore, there is very little difference in the linear wave frequency over the perpendicular range of the simulation between $m_i/m_e = 36$ and $m_i/m_e = 1836$.

The noticeable difference between the two cases arises in the electron collisionless

damping rate γ_e/ω in Fig. 14(b). The ion damping is slightly smaller for the realistic mass ratio relative to the reduced mass ratio, but the electron damping drops by nearly an order of magnitude. Other than the amplitude changes, however, the individual species damping rates γ_s/ω on a log-log plot have the same the functional form, only a different relative weighting. The reduced mass ratio case has nearly a factor of ten larger relative contribution to the collisionless damping than the realistic mass ratio. Note that significant collisionless damping of a wave occurs when $\gamma/\omega \gtrsim 0.1$ (marked by a horizontal dashed line), so total collisionless damping is relatively weak over the perpendicular range of the simulation for a realistic mass ratio $m_i/m_e = 1836$, whereas the damping is very strong with $\gamma_{tot}/\omega \sim 1.0$ at the smallest perpendicular scales for the reduced mass ratio $m_i/m_e = 36$. This enables collisionless damping to remove energy from the turbulent fluctuations completely over the resolve range of scales, avoiding any problematic bottlenecks at the smallest scales.

Note that reducing the mass ratio to values $m_i/m_e < 32$ (not shown) leads to a significant qualitative change from the behavior of the collisionless damping shown here. At these very low mass ratio values, the ion collisionless damping does not drop off at $k_\perp \rho_i \gg 1$, potentially leading to qualitatively incorrect results about the relative ion and electron damping (Klein *et al.* 2017).

Appendix B. Particle Energization by Component and Species

In the Vlasov-Maxwell system of equations, the rate of change of particle energy density at a given position in space is given by the rate of electromagnetic work, $\mathbf{j}\cdot\mathbf{E}$ (Klein *et al.* 2017), confirming the familiar concept the only the electric field can change the energy of charged particles. In the low-frequency limit of kinetic plasma theory, one may average the Vlasov-Maxwell equations over the gyrophase θ in cylindrical velocity space $(v_\parallel, v_\perp, \theta)$ to obtain the reduced system of gyrokinetics (Frieman & Chen 1982; Howes *et al.* 2006). The benefit of this procedure is the reduction of velocity space to two dimensions $(v_\parallel, v_\perp)$ at the expense of discarding the physics at cyclotron frequencies and higher; effectively, the cyclotron resonances and fast magnetosonic waves are eliminated, while retaining finite Larmor radius effects and collisionless damping via the Landau resonance.

In addition to this elimination of the cyclotron resonances, a component of the perpendicular electromagnetic work, $\mathbf{j}_\perp \cdot \mathbf{E}_\perp$ is alternatively expressed in terms of the magnetic mirror force, $\mathbf{F}_{mir} = -\mu\nabla_\parallel|\mathbf{B}|$, where the magnetic moment of a particle is given by $\mu_s = m_s v_\perp^2/2|B|$. In the anisotropic limit $k_\parallel \ll k_\perp$ of the gyrokinetic approximation, the change in the magnetic field magnitude is dominated by the variation in the parallel component of the field, $\delta|\mathbf{B}| = \delta B_\parallel + \mathcal{O}(|\delta\mathbf{B}|^2)$. For electromagnetic waves with a fluctuation in the magnetic field strength, the magnetic mirror force $-\mu\nabla_\parallel\delta B_\parallel$ acting on the magnetic moment μ of the particle gyromotion, leads to collisionless damping of the wave via the Landau resonance, a process denoted by the term transit-time damping, or alternatively called Barnes damping (Barnes 1966; Quataert 1998).

The bottom line is in gyrokinetics there are two separate mechanisms that can lead to resonant collisionless particle energization: Landau damping mediated by the parallel electric field $E_\parallel$ and transit-time damping mediated by gradients in the parallel magnetic field perturbation $\nabla_\parallel\delta B_\parallel$. In this paper, we focus solely on the particle energization by Landau damping through the parallel electric field $E_\parallel$, leaving a detailed analysis of transit-time damping to future work.

Although gyrokinetics eliminates cyclotron resonant heating, it still describes the electromagnetic work done by all three components of $\mathbf{j}\cdot\mathbf{E}$. The primary focus of this paper is resonant heating by Landau damping through the parallel electric field $E_\parallel$, so plots in

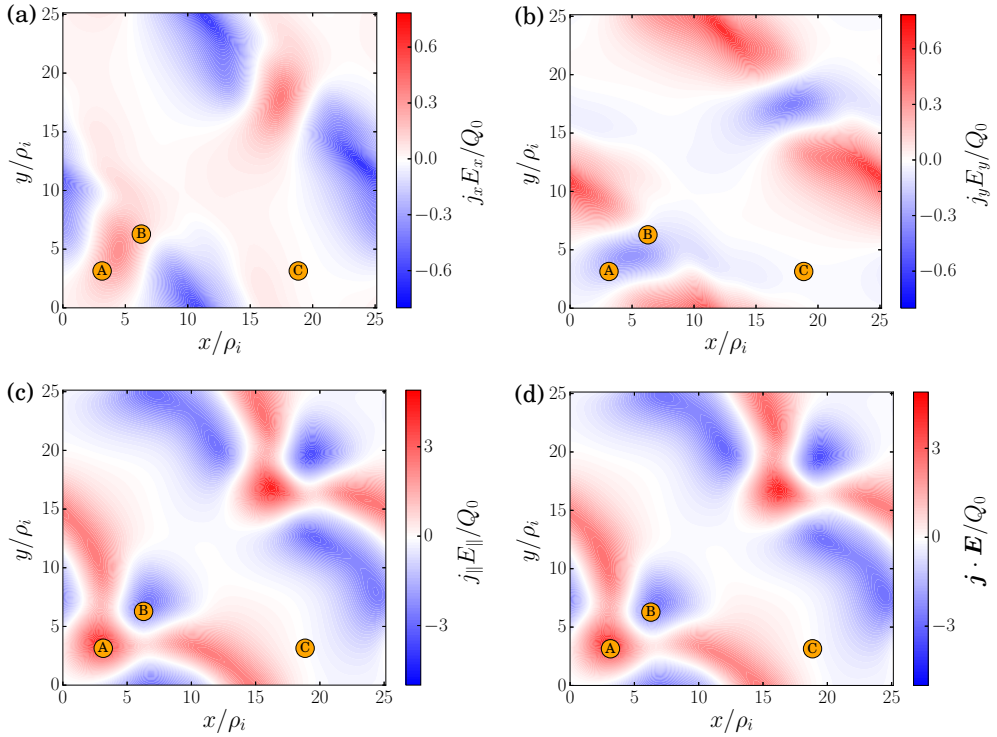


FIGURE 15. Plots of the different components of the electromagnetic work (a) $\langle j_x E_x\rangle_\tau$, (b) $\langle j_y E_y\rangle_\tau$, and (c) $\langle j_\parallel E_\parallel\rangle_\tau$, as well as the total work (d) $\langle \mathbf{j}\cdot\mathbf{E}\rangle_\tau$ averaged over a single wave period $\tau = 0.992T_0$ centered at time $t/T_0 = 1.86$.

the body of paper focus only on the parallel contribution $j_\parallel E_\parallel$. In Fig. 15, we present here for completeness the three components of the electromagnetic work (a) $\langle j_x E_x\rangle_\tau$, (b) $\langle j_y E_y\rangle_\tau$, and (c) $\langle j_\parallel E_\parallel\rangle_\tau$ averaged over single wave period $\tau = 0.992T_0$ centered at time $t/T_0 = 1.86$. The components $j_x E_x$ and $j_y E_y$ dominantly represent the energy transfer between fields and particles associated with undamped wave motion, for example representing magnetic tension as the restoring force for the Alfvén wave. Therefore, $j_x E_x$ and $j_y E_y$ represent oscillatory energy transfer, and averaged over one wave period there is very little net energy change. By comparison, the single-wave period averaged $\langle j_\parallel E_\parallel\rangle_\tau$ represents the secular energy transfer associated with collisionless damping,is much larger than that for $j_x E_x$ or $j_y E_y$. Note that (d) the total single-wave period averaged total electromagnetic work $\langle \mathbf{j}\cdot\mathbf{E}\rangle_\tau$ is dominated by the parallel component $\langle j_\parallel E_\parallel\rangle_\tau$. This comparison motivates our focus in the body of this paper on the parallel contribution to the electromagnetic work, $j_\parallel E_\parallel$.

We also plot separately the parallel electromagnetic work on the ions $j_{\parallel,i}E_\parallel$ in Fig. 16 and on the electrons $j_{\parallel,e}E_\parallel$ in Fig. 17. The spatial patterns of the instantaneous rate of work at $t/T_0 =$ (a) 1.75, (b) 1.86, and (c) 2.03, as well as (d) the $\langle j_{\parallel,s}E_\parallel\rangle_\tau$ averaged over one full wave period $\tau = 0.992T_0$ centered at time $t/T_0 = 1.86$, are similar for both species, but the rate of electron energization in this plane is about twice the magnitude of that for the ions. Since the ion and electron linear damping rates are similar for $k_\perp\rho_i \lesssim 1$, this may suggest significant energy removal at higher $k_\perp\rho_i > 1$ where electrons are expected to receive a greater share of the removed turbulent energy. A future examination

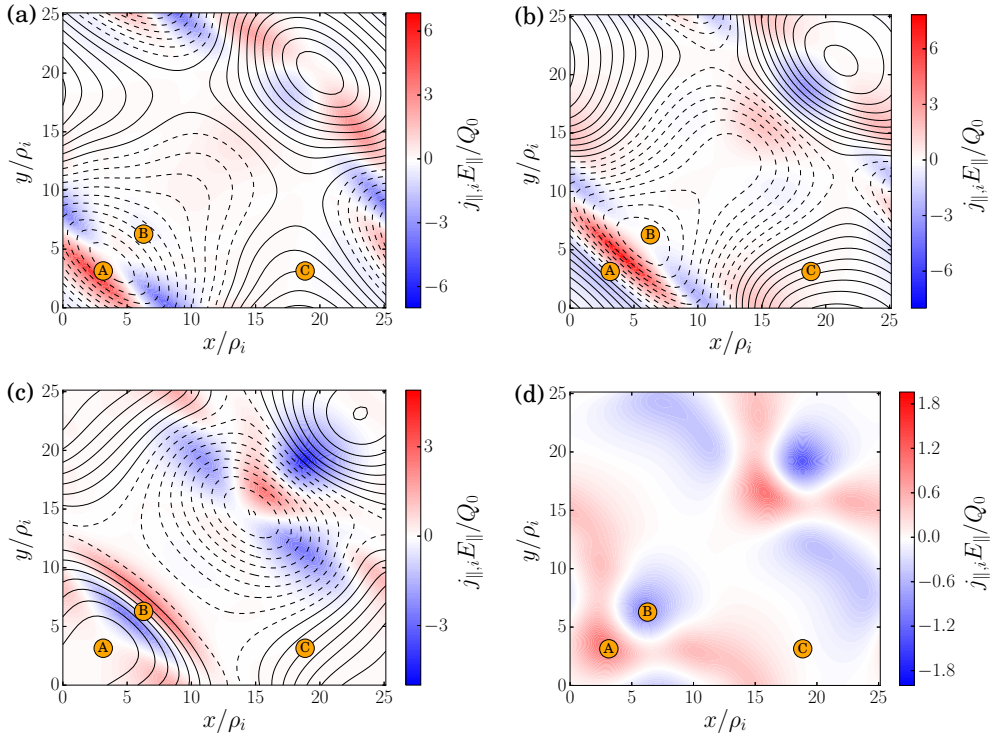


FIGURE 16. Plots of the instantaneous rate of parallel electromagnetic work on the ions $j_{\parallel,i}E_\parallel$ and contours of the parallel vector potential $A_\parallel$ (contours, positive solid, negative dashed) at times $t/T_0 =$ (a) 1.75, (b) 1.86, and (c) 2.03, as well as (d) $\langle j_{\parallel,i}E_\parallel\rangle_\tau$ averaged over one full wave period $\tau = 0.992T_0$ centered at time $t/T_0 = 1.86$.

of the ion and electron energization will investigate the typical length scale at which particles are energized in more detail.

REFERENCES

ABEL, I. G., BARNES, M., COWLEY, S. C., DORLAND, W. & SCHEKOCHIHIN, A. A. 2008 Linearized model Fokker-Planck collision operators for gyrokinetic simulations. I. Theory. *Phys. Plasmas* **15** (12), 122509.

BARNES, A. 1966 Collisionless Damping of Hydromagnetic Waves. *Phys. Fluids* **9**, 1483–1495.

BARNES, M., ABEL, I. G., DORLAND, W., ERNST, D. R., HAMMETT, G. W., RICCI, P., ROGERS, B. N., SCHEKOCHIHIN, A. A. & TATSUNO, T. 2009 Linearized model Fokker-Planck collision operators for gyrokinetic simulations. II. Numerical implementation and tests. *Phys. Plasmas* **16** (7), 072107.

BOLDYREV, S. 2006 Spectrum of Magnetohydrodynamic Turbulence. *Phys. Rev. Lett.* **96** (11), 115002.

BOROVSKY, J. E. & DENTON, M. H. 2011 No Evidence for Heating of the Solar Wind at Strong Current Sheets. *Astrophys. J. Lett.* **739**, L61.

BRANDENBURG, A. 2014 Magnetic Prandtl Number Dependence of the Kinetic-to-magnetic Dissipation Ratio. *Astrophys. J.* **791**, 12.

BRIZARD, A. J. & HAHM, T. S. 2007 Foundations of nonlinear gyrokinetic theory. *Rev. Mod. Phys.* **79**, 421–468.

DORLAND, W. & HAMMETT, G. W. 1993 Gyrofluid turbulence models with kinetic effects. *Phys. Fluids B* **5**, 812–835.

DRAKE, D. J., SCHROEDER, J. W. R., HOWES, G. G., KLETZING, C. A., SKIFF, F., CARTER,

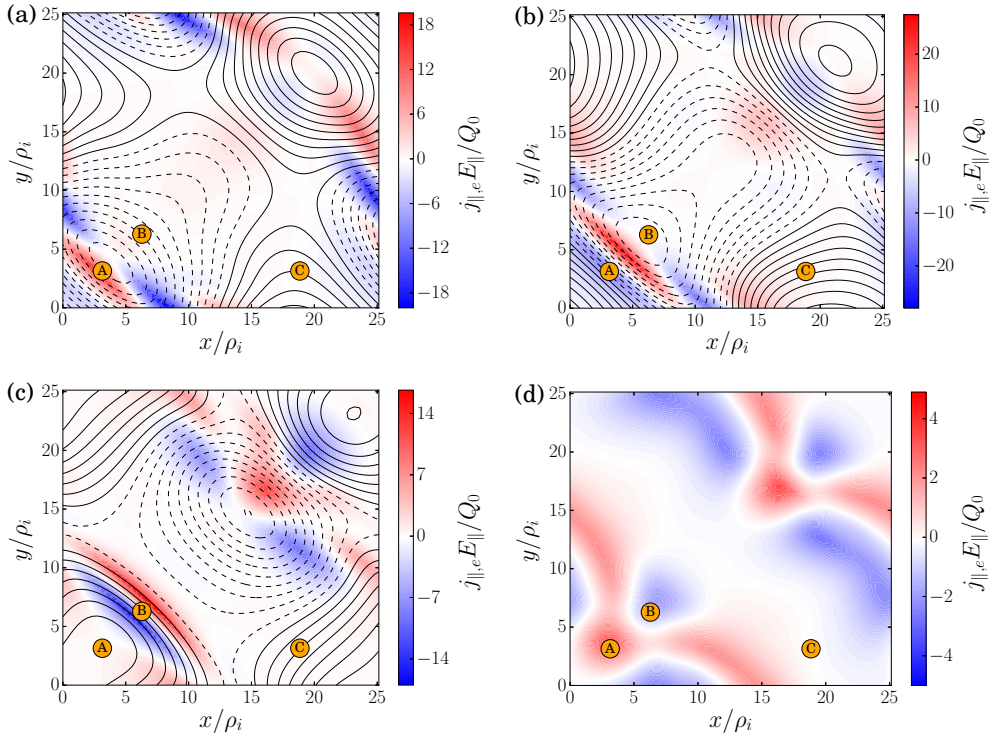


FIGURE 17. Plots of the instantaneous rate of parallel electromagnetic work on the electrons $j_{\parallel,e}E_\parallel$ and contours of the parallel vector potential $A_\parallel$ (contours, positive solid, negative dashed) at times $t/T_0 =$ (a) 1.75, (b) 1.86, and (c) 2.03, as well as (d) $\langle j_{\parallel,e}E_\parallel\rangle_\tau$ averaged over one full wave period $\tau = 0.992T_0$ centered at time $t/T_0 = 1.86$.

T. A. & AUERBACH, D. W. 2013 Alfvén wave collisions, the fundamental building block of plasma turbulence. IV. Laboratory experiment. *Physics of Plasmas* **20** (7), 072901.

ELSASSER, W. M. 1950 The Hydromagnetic Equations. *Physical Review* **79**, 183.

FRIEMAN, E. A. & CHEN, L. 1982 Nonlinear gyrokinetic equations for low-frequency electromagnetic waves in general plasma equilibria. *Phys. Fluids* **25**, 502–508.

GALTIER, S., NAZARENKO, S. V., NEWELL, A. C. & POUQUET, A. 2000 A weak turbulence theory for incompressible magnetohydrodynamics. *J. Plasma Phys.* **63**, 447–488.

GOLDREICH, P. & SRIDHAR, S. 1995 Toward a Theory of Interstellar Turbulence II. Strong Alfvénic Turbulence. *Astrophys. J.* **438**, 763–775.

HOWES, G. G. 2008 Inertial range turbulence in kinetic plasmas. *Phys. Plasmas* **15** (5), 055904.

HOWES, G. G. 2015 A dynamical model of plasma turbulence in the solar wind. *Philosophical Transactions of the Royal Society of London A: Mathematical, Physical and Engineering Sciences* **373** (2041), 20140145.

HOWES, G. G. 2016 The Dynamical Generation of Current Sheets in Astrophysical Plasma Turbulence. *Astrophys. J. Lett.* **82**, L28.

HOWES, G. G. 2017 A prospectus on kinetic heliophysics. *Physics of Plasmas* **24** (5), 055907.

HOWES, G. G., COWLEY, S. C., DORLAND, W., HAMMETT, G. W., QUATAERT, E. & SCHEKOCHIHIN, A. A. 2006 Astrophysical Gyrokinetics: Basic Equations and Linear Theory. *Astrophys. J.* **651**, 590–614.

HOWES, G. G., DRAKE, D. J., NIELSON, K. D., CARTER, T. A., KLETZING, C. A. & SKIFF, F. 2012 Toward Astrophysical Turbulence in the Laboratory. *Phys. Rev. Lett.* **109** (25), 255001.

HOWES, G. G., KLEIN, K. G. & LI, T. C. 2017 Diagnosing Collisionless Energy Transfer Using Wave-Particle Correlations: Vlasov-Poisson Plasmas. *J. Plasma Phys.* **83** (1), 705830102.

Howes, G. G., Klein, K. G. & TenBarge, J. M. 2014 Validity of the Taylor Hypothesis for Linear Kinetic Waves in the Weakly Collisional Solar Wind. *Astrophys. J.* **789**, 106.

Howes, G. G. & Nielson, K. D. 2013 Alfvén wave collisions, the fundamental building block of plasma turbulence. I. Asymptotic solution. *Phys. Plasmas* **20** (7), 072302.

Howes, G. G., Nielson, K. D., Drake, D. J., Schroeder, J. W. R., Skiff, F., Kletzing, C. A. & Carter, T. A. 2013 Alfvén wave collisions, the fundamental building block of plasma turbulence. III. Theory for experimental design. *Physics of Plasmas* **20** (7), 072304.

Iroshnikov, R. S. 1963 The turbulence of a conducting fluid in a strong magnetic field. *Astron. Zh.* **40**, 742, English Translation: Sov. Astron., 7 566 (1964).

Karimabadi, H., Roytershteyn, V., Wan, M., Matthaeus, W. H., Daughton, W., Wu, P., Shay, M., Loring, B., Borovsky, J., Leonardis, E., Chapman, S. C. & Nakamura, T. K. M. 2013 Coherent structures, intermittent turbulence, and dissipation in high-temperature plasmas. *Phys. Plasmas* **20** (1), 012303.

Kawamori, E. 2013 Experimental Verification of Entropy Cascade in Two-Dimensional Electrostatic Turbulence in Magnetized Plasma. *Phys. Rev. Lett.* **110** (9), 095001.

Klein, K. G. 2017 Characterizing fluid and kinetic instabilities using field-particle correlations on single-point time series. *Phys. Plasmas* **24** (5), 055901.

Klein, K. G. & Howes, G. G. 2015 Predicted impacts of proton temperature anisotropy on solar wind turbulence. *Phys. Plasmas* **22** (3), 032903.

Klein, K. G. & Howes, G. G. 2016 Measuring Collisionless Damping in Heliospheric Plasmas using Field-Particle Correlations. *Astrophys. J. Lett.* **826**, L30.

Klein, K. G., Howes, G. G. & TenBarge, J. M. 2017 Diagnosing collisionless energy transfer using field-particle correlations: gyrokinetic turbulence. *J. Plasma Phys.* In press.

Kraichnan, R. H. 1965 Inertial range spectrum of hyromagnetic turbulence. *Phys. Fluids* **8**, 1385–1387.

Kruskal, M. D. & Oberman, C. R. 1958 On the Stability of Plasma in Static Equilibrium. *Phys. Fluids* **1**, 275–280.

Kulsrud, R. M. 1983 MHD description of plasma. In *Basic Plasma Physics I* (ed. A. A. Galeev & R. N. Sudan), *Handbook of Plasma Physics*, vol. 1, chap. 1.4, pp. 115–145. North Holland.

Li, T. C., Howes, G. G., Klein, K. G. & TenBarge, J. M. 2016 Energy Dissipation and Landau Damping in Two- and Three-dimensional Plasma Turbulence. *Astrophys. J. Lett.* **832**, L24.

Matthaeus, W. H. & Montgomery, D. 1980 Selective decay hypothesis at high mechanical and magnetic Reynolds numbers. *Annals of the New York Academy of Sciences* **357**, 203–222.

Meneguzzi, M., Frisch, U. & Pouquet, A. 1981 Helical and nonhelical turbulent dynamos. *Phys. Rev. Lett.* **47**, 1060–1064.

Morrison, P. J. 1994 The energy of perturbations for Vlasov plasmas. *Phys. Plasmas* **1**, 1447–1451.

Navarro, A. B., Teaca, B., Told, D., Groselj, D., Crandall, P. & Jenko, F. 2016 Structure of Plasma Heating in Gyrokinetic Alfvénic Turbulence. *Physical Review Letters* **117** (24), 245101.

Ng, C. S. & Bhattacharjee, A. 1996 Interaction of Shear-Alfven Wave Packets: Implication for Weak Magnetohydrodynamic Turbulence in Astrophysical Plasmas. *Astrophys. J.* **465**, 845.

Nielson, K. D., Howes, G. G. & Dorland, W. 2013 Alfvén wave collisions, the fundamental building block of plasma turbulence. II. Numerical solution. *Physics of Plasmas* **20** (7), 072303.

Numata, R., Howes, G. G., Tatsuno, T., Barnes, M. & Dorland, W. 2010 AstroGK: Astrophysical gyrokinetics code. *J. Comp. Phys.* **229**, 9347.

Osman, K. T., Matthaeus, W. H., Gosling, J. T., Greco, A., Servidio, S., Hnat, B., Chapman, S. C. & Phan, T. D. 2014 Magnetic Reconnection and Intermittent Turbulence in the Solar Wind. *Phys. Rev. Lett.* **112** (21), 215002.

Osman, K. T., Matthaeus, W. H., Greco, A. & Servidio, S. 2011 Evidence for Inhomogeneous Heating in the Solar Wind. *Astrophys. J. Lett.* **727**, L11.

Osman, K. T., Matthaeus, W. H., Wan, M. & Rappazzo, A. F. 2012 Intermittency and Local Heating in the Solar Wind. *Phys. Rev. Lett.* **108** (26), 261102.

Parker, E. N. 1958 Dynamics of the Interplanetary Gas and Magnetic Fields. *Astrophys. J.* **128**, 664.

Parker, J. T., Highcock, E. G., Schekochihin, A. A. & Dellar, P. J. 2016 Suppression of phase mixing in drift-kinetic plasma turbulence. *Phys. Plasmas* **23** (7), 070703.

Perri, S., Goldstein, M. L., Dorelli, J. C. & Sahraoui, F. 2012 Detection of Small-Scale Structures in the Dissipation Regime of Solar-Wind Turbulence. *Phys. Rev. Lett.* **109** (19), 191101.

Plunk, G. G. 2013 Landau damping in a turbulent setting. *Phys. Plasmas* **20** (3), 032304.

Plunk, G. G., Cowley, S. C., Schekochihin, A. A. & Tatsuno, T. 2010 Two-dimensional gyrokinetic turbulence. *Journal of Fluid Mechanics* **664**, 407–435.

Plunk, G. G. & Tatsuno, T. 2011 Energy Transfer and Dual Cascade in Kinetic Magnetized Plasma Turbulence. *Phys. Rev. Lett.* **106** (16), 165003.

Quataert, E. 1998 Particle Heating by Alfvénic Turbulence in Hot Accretion Flows. *Astrophys. J.* **500**, 978–991.

Schekochihin, A. A., Cowley, S. C., Dorland, W., Hammett, G. W., Howes, G. G., Quataert, E. & Tatsuno, T. 2009 Astrophysical Gyrokinetics: Kinetic and Fluid Turbulent Cascades in Magnetized Weakly Collisional Plasmas. *Astrophys. J. Supp.* **182**, 310–377.

Schekochihin, A. A., Parker, J. T., Highcock, E. G., Dellar, P. J., Dorland, W. & Hammett, G. W. 2016 Phase mixing versus nonlinear advection in drift-kinetic plasma turbulence. *J. Plasma Phys.* **82** (2), 905820212.

Spitzer, L. 1962 *Physics of Fully Ionized Gases*. Physics of Fully Ionized Gases, New York: Interscience (2nd edition), 1962.

Sridhar, S. & Goldreich, P. 1994 Toward a theory of interstellar turbulence. 1: Weak Alfvenic turbulence. *Astrophys. J.* **432**, 612–621.

Tatsuno, T., Schekochihin, A. A., Dorland, W., Plunk, G., Barnes, M. A., Cowley, S. C. & Howes, G. G. 2009 Nonlinear phase mixing and phase-space cascade of entropy in gyrokinetic plasma turbulence. *Phys. Rev. Lett.* **103** (1), 015003.

TenBarge, J. M., Daughton, W., Karimabadi, H., Howes, G. G. & Dorland, W. 2014 Collisionless reconnection in the large guide field regime: Gyrokinetic versus particle-in-cell simulations. *Phys. Plasmas* **21** (2), 020708.

TenBarge, J. M. & Howes, G. G. 2013 Current Sheets and Collisionless Damping in Kinetic Plasma Turbulence. *Astrophys. J. Lett.* **771**, L27.

Uritsky, V. M., Pouquet, A., Rosenberg, D., Mininni, P. D. & Donovan, E. F. 2010 Structures in magnetohydrodynamic turbulence: Detection and scaling. *Phys. Rev. E* **82** (5), 056326.

Verniero, J. L. & Howes, G. G. 2017 The Physics of Energy Transfer in Alfvén wave collisions: Periodic Plane Waves vs. Isolated Wavepackets. *J. Plasma Phys.* In preparation.

Verniero, J. L., Howes, G. G. & Klein, K. G. 2017 Nonlinear energy transfer and current sheet development in localized Alfvén wavepacket collisions in the strong turbulence limit. *J. Plasma Phys.* Submitted.

Wan, M., Matthaeus, W. H., Karimabadi, H., Roytershteyn, V., Shay, M., Wu, P., Daughton, W., Loring, B. & Chapman, S. C. 2012 Intermittent Dissipation at Kinetic Scales in Collisionless Plasma Turbulence. *Phys. Rev. Lett.* **109** (19), 195001.

Wang, X., Tu, C., He, J., Marsch, E. & Wang, L. 2013 On Intermittent Turbulence Heating of the Solar Wind: Differences between Tangential and Rotational Discontinuities. *Astrophys. J. Lett.* **772**, L14.

Wu, P., Perri, S., Osman, K., Wan, M., Matthaeus, W. H., Shay, M. A., Goldstein, M. L., Karimabadi, H. & Chapman, S. 2013 Intermittent Heating in Solar Wind and Kinetic Simulations. *Astrophys. J. Lett.* **763**, L30.

Zhdankin, V., Uzdensky, D. A. & Boldyrev, S. 2015 Temporal Analysis of Dissipative Structures in Magnetohydrodynamic Turbulence. *Astrophys. J.* **811**, 6.

Zhdankin, V., Uzdensky, D. A., Perez, J. C. & Boldyrev, S. 2013 Statistical Analysis of Current Sheets in Three-dimensional Magnetohydrodynamic Turbulence. *Astrophys. J.* **771**, 124.